Marine Pollution Bulletin
June 2022, Volume 179 Pages 113748 (17p.)
https://doi.org/10.1016/j.marpolbul.2022.113748
https://archimer.ifremer.fr/doc/00772/88372/

Periodicity of wave-driven flows and lagoon water renewal for 74 Central Pacific Ocean atolls

Andréfouët Serge [1, *], Desclaux Terence [4], Buttin Julie [1], Jullien Swen [2], Aucan Jérôme [3], Le Gendre Romain [4], Liao Vetea [5]

[1] Institut de Recherche pour le Développement, UMR 9220 ENTROPIE (Institut de Recherche Pour le Développement), Université de la Réunion, Université de Nouvelle-Calédonie, Ifremer, Centre National de la Recherche Scientifique, BP A5, 98848 Nouméa cedex, New Caledonia
[2] Ifremer, Univ. Brest, CNRS, IRD, Laboratoire d'Océanographie Physique et Spatiale (LOPS), IUEM, Plouzané, France
[3] IRD, LOCEAN (UMR 7159), BP A5, 98848 Nouméa cedex, New Caledonia
[4] IFREMER, ENTROPIE, UMR 9220, Institut de Recherche pour le Développement, Université de la Réunion, Université de Nouvelle-Calédonie, Ifremer, Centre National de la Recherche Scientifique, BP 32078, 98897 Noumea Cedex, New Caledonia
[5] Direction des Ressources Marines, BP 20, 98713 Papeete, French Polynesia

* Corresponding author : Serge Andréfouët, email address : serge.andrefouet@ird.fr

Abstract :

French Polynesia atolls are spread on a vast 2300 by 1200 km Central Pacific Ocean area exposed to spatially and temporally dependent wave forcing. They also have a wide range of closed to open morphologies and several have been suitable to develop from black-lipped pearl oysters a substantial pearl farming activity in the past 30 years, representing nowadays the 2nd source of income for French Polynesia. Considering here only the component of lagoon renewal that is driven by waves, we investigate for 74 atolls different lagoon renewal metrics using 20 years of wave model data at 0.05° spatial resolution. Wavelet spectral analyses highlight that atolls, even in close vicinity, can be exposed to different and characteristic periodicities in wave-driven flows and water renewal. These characteristics are discussed in relation to pearl farming atolls, including atolls known to be efficient oyster spat producers, a critical activity for pearl farming sustainability.

Highlights

► The wave-driven lagoon renewal is investigated for 74 atolls. ► Cross-rims flows and lagoon renewal are computed from 20 years of wave data. ► Wavelet analysis highlights the time periodicity of renewal for each atoll. ► Periodicity differs between atolls. ► The case of pearl farming atolls are discussed.

Keywords : Tuamotu, Pearl farming, WaveWatch III, Hoa, Residence time, Wavelet transform

Introduction

Atolls are one of the major geomorphological types of coral reefs (Woodroffe and Biribo 2011), characterized by an inner lagoon surrounded by a carbonate rim, which is itself often capped by reef islands of a few meters elevation. Atolls are particularly present in the Pacific and Indian oceans, with several countries and territories made of atolls only (Maldives, the British Indian Ocean Territories, Tuvalu, Marshall Islands, Tokelau). The most recent published list of atolls reported 439 atolls worldwide (Goldberg 2016), although this number is currently under revision with quantitative geomorphological criteria, and is currently higher than 600 (Andréfouët et al. in prep.) The largest group of atolls worldwide is found in French Polynesia, with 84 atolls, although 4 of the smallest ones have a dry lagoon and one is uplifted (Andréfouët and Adjeroud 2018). The Tuamotu-Gambier Archipelago alone has 72 atolls with lagoon. In Tuamotu-Gambier, the atoll lagoon morphological diversity is substantial with a large range of size (from 2 to 1700 km^2), depth (maximum depth from 2 to 70 meters), and degree of aperture (from 0 to 76%) (Andréfouët et al. 2001a, Andréfouët et al. 2005, Andréfouët et al. 2020). The degree of aperture of an atoll was considered to be the ratio between (i) the sum of the width of all hydrodynamically efficient channels deep enough to let oceanic water circulating towards the lagoon and (ii) the perimeter of the atoll (Andréfouët et al. 2001a). This water can enter the lagoon through 1) deep passes during incoming tides, although not all atolls have such passages; 2) shallow (few centimeters to 2m depth at most) channels called *hoa* which can be bounded by reef islands, conglomerate and sand banks (Stoddart and Forberg 1994, Kench and MacLean 2004, Tartinville and Rancher 2000). The incoming flow through *hoa* is driven by tide and waves (Aucan et al. 2021). In Ahe atoll, residual (tide-filtered) flow through the pass were always outgoing and corresponded to the volume of water entering through the *hoa* (Dumas et al. 2012). Unlike passes, *hoa* are found on most atolls but their numbers, width, and morphology also vary greatly between atolls, and between atoll rim sectors within an atoll (Andréfouët et al. 2001a).

Due to their wide range of morphologies, not all French Polynesia atolls are equal, or have the same potential to sustain population livelihoods with natural resources or commercial activities. Inhabited atolls with productive enough lagoons are better suited for fisheries and mariculture developments. Mariculture, and in particular the production of black pearls, is a significant industry in French Polynesia. It was the second source of incomes for the country, after tourism, at least until 2019 before the covid-19 pandemic. While many atolls are clearly unsuitable for pearl farming due to their shallowness, or lack of *Pinctada margaritifera* black lipped pearl oyster population from which black pearls are produced, about 30 atolls have accommodated pearl farming activities in the past 40 years, with various levels of success and problems. In 2019, 25 Tuamotu-Gambier atolls had some activities, but most of the production came from 12 atolls, with a production between 87 kg and 3300 kg of pearls (DRM 2019). Among the problems, mass mortality events have impacted oyster population, natural or farmed, and pearl production. These mass mortality events are likely due to algal blooms

like in Takaroa in 2013 (Rodier et al. 2019), and can be related to dystrophy, anoxia and thermal stress. These processes can be related to an unusually long rupture of incoming water flow from the ocean to the lagoon, leading to very poor water renewal. Andréfouët et al. (2015) investigated the few known periods of mass mortalities and concluded that a combination of very local low wind, high temperature and low swell could explain these events. Some atolls seem more susceptible to mortalities than others, in particular Ahe, Takaroa, Takapoto, Manihi, Hikueru and Manihiki (the latter is a pearl farming in Cook Islands) (Andréfouët et al. 2015).

Pearl farming atolls are also characterized by different activities. Some atolls have been used in particular for spat collecting. Unfortunately, farmers do not provide, or even record, their spat collecting results even today after 30 years or more of practice, but Ahe, Manihi, Takaroa, Takapoto atolls have been consistently very productive, except after mass mortality events, like Takaroa. Other atolls are also spat collector atolls but far less effectively (Table 1). This activity forms the foundation of the industry, as it provides the farmed stock of *Pinctada margaritifera*, from which pearls can be produced. Other farming atolls can be specialized on pearl production, and may import spats to achieve their goals. Spat collecting is inherently a complex biophysical-driven process, but which natural factors affect the potential of an atoll to be a consistently good spat producer is unclear. The drivers can be a combination of: the oyster populations, the planktonic food web that is favorable to adult growth and larvae survival, the atoll geomorphology, and the hydrodynamics of the lagoon in particular its flushing and renewal. These drivers are not independent of each other (Dufour et al. 2001). Delesalle and Sournia (1992) could empirically demonstrate a linear relationship between phytoplankton biomass (chlorophyll *a* concentration) and residence time in tropical lagoons. In Tuamotu atolls, Andréfouët et al. (2001b) confirmed a linear relationship between concurrent measured phytoplanktonic standing stocks and estimated renewal times for 19 atolls, pending at least 2 different groups of atolls were considered, based on their sizes (larger or smaller than 25km^2). Building on Tartinville and Rancher (2000), the renewal time in Andréfouët et al. (2001b) could be computed using 1) significant wave height measured along satellite altimetry tracks; 2) same day simultaneous flows in *hoa* providing an empirical wave height *vs* flow relationship; 3) atolls degree of aperture; and 4) an estimate of the lagoon volumes. The altimetry data set was at that time (2 decades ago) too restricted, spatially and temporally, to provide continuous daily series of flows and renewal but the authors concluded that it would be very relevant to provide a combined trophic-hydrodynamic signature of lagoons using a temporal spectrum of renewal times. Specific renewal behaviors or renewal anomalies could be detected and potentially related to, for instance, susceptibility in mass mortality events, or potential for spat collecting.

Today, the situation is different, and we can take advantage of extensive gridded wave datasets to revisit the idea of computing the spectrum of renewal times for as many atolls as possible, including

all possible atoll morphologies. However, while it would be ideal to include all the processes known to drive a lagoon water renewal, this is not possible with the current level of knowledge and geomorphological characterization of most atolls. Indeed, few Tuamotu atolls have been instrumented to measure currents across their lagoon boundaries, in *hoa* or passes (Lenhardt 1992, Dumas et al. 2012, Aucan et al. 2021). Furthermore, the bathymetry of only a handful of deep passes have been precisely mapped (Andréfouët et al. 2020). These gaps prevent in particular a good characterization and generalization of the flows (in or out) through these passes, which is primarily tide-driven (Dumas et al. 2012). In fact, to model lagoon renewal processes for all French Polynesia atolls without new specific atoll-dependent field work, there is currently enough knowledge only to describe the inflow driven by waves across the shallow *hoa*. Therefore, for a multi-atoll renewal comparison, we focus hereafter on this aspect. Since only one aspect of the renewal processes will be treated here, we follow Lucas and Deleersnijder (2020) in qualifying this work of a non-holistic but rather an atomistic approach of modelling water processes in semi-closed coastal ecosystems.

The present study investigates for 74 atolls the daily wave-driven inflow forced by a wave simulation over a 20-year period. To normalize the effects of this inflow for different lagoon sizes and volumes, a renewal time (based on the total volume if it is known), and a 'surface renewal time' (based on the volume of the first meter of the lagoon) are computed at daily scale. The temporal scales (longer than a day) of wave-driven flows and renewal times are analyzed for each atoll using a wavelet decomposition, and different groups of atolls are evidenced. This first approach considers daily instantaneous indicators that ignore the recent or distant past. A time-integrated metric of renewal is thus also computed to provide a lagoon water age metric accounting for the succession of wave-driven inflows. Water flows, renewal times (volumic or sub-volumic), and aging are discussed relative to their bias and interests in particular in the context of pearl farming activity.

Material and methods

Study sites

This study investigated 74 French Polynesia atolls (Fig. 1), selected considering the availability of satellite imagery (see below). From the 72 Tuamotu and Gambier atolls that have a lagoon, 69 are considered here. In addition, five atolls from the Society Archipelago were included. The main known characteristics of all these atolls are provided in Table 1. They cover an extensive 2300 by 1200 km region oceanic area, and are therefore exposed to wave regimes that are modulated by their geographic position and their relative position to each other, as waves can be obstructed by nearby atolls (Andréfouët et al. 2012; Dutheil et al. 2021).

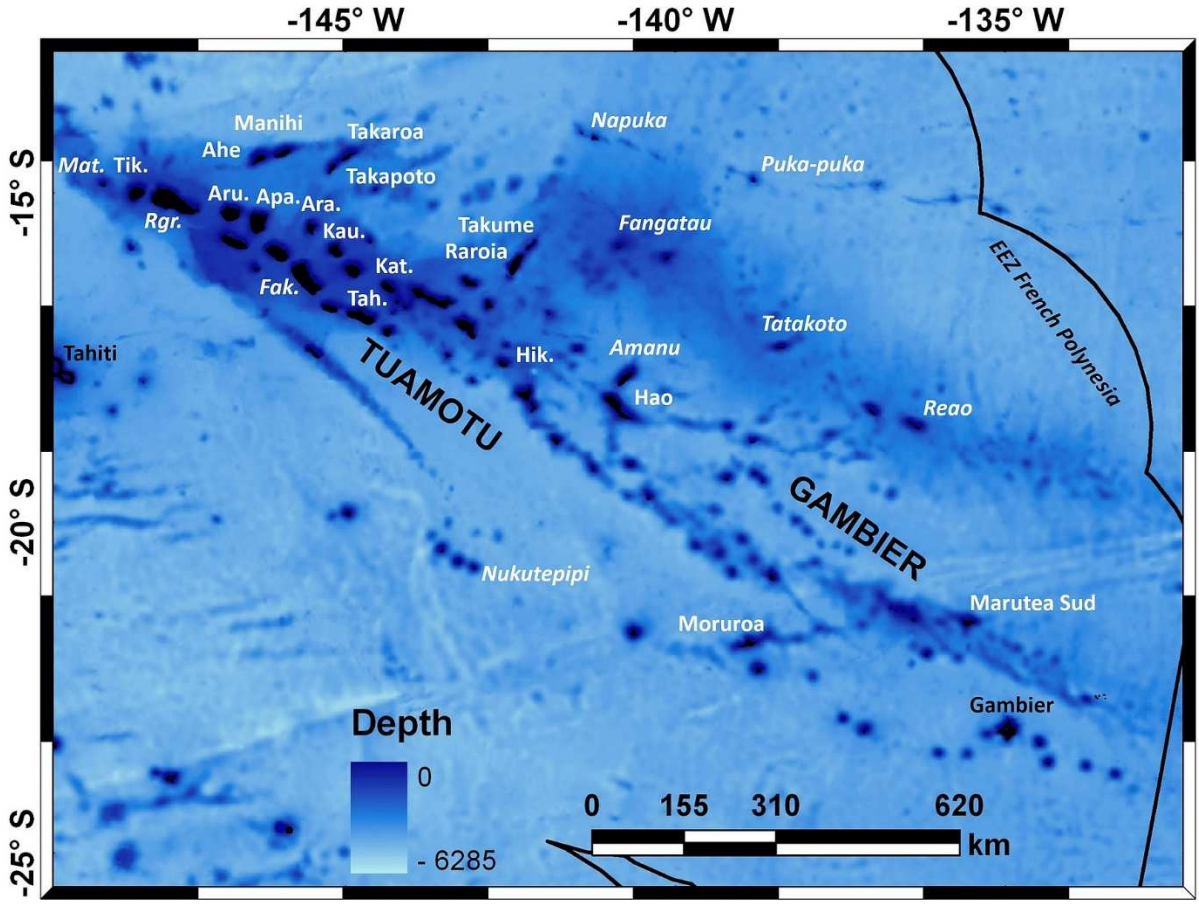

Figure 1: Bathymetric map of the studied area and location of the studied atolls in Tuamotu-Gambier archipelagoes (5 Society Archipelago atolls are not shown). Atolls mentioned in the text are shown in white normal font. Atolls frequently studied in recent scientific literature but not named here except in Table 1 are in italics. Names in black font are high islands. For names abbreviated for better visibility: Apa.=Apataki, Ara.=Aratika, Aru.=Arutua, Fak.=Fakarava, Hik.=Hikueru. Kat.=Katiu, Kau.=Kauehi, Mat.=Mataiva, Tah.=Tahanea, Tik.=Tikehau.

Aperture of atoll rims

Andréfouët et al (2001a) described 9 types of atoll rims in the Tuamotu Archipelago. These rim types were related to the abundance of four types of cover, namely vegetation, carbonate conglomerate, intertidal areas, and water in *hoa*. Several of these rim types can be related to the complete absence of *hoa* (rim types 1, 8, 9), or to different *hoa* morphologies (rim types 2, 3, 4, 5, 6, and 7). The *hoa* morphology depends on its borders, either formed by soft sediments that can be widely displaced (coral sand, rubble, and small boulders accumulation; present on rim types 2, 3, 4, 6, 7), or hard lithified coral conglomerate that are stable but eroded at the limit of the water (Montaggioni and Pirrazoli 1994; present on rim types 2, 5, 7). The rim type 4 is made of wide *hoa*, similar to reef flats that can be completely submerged and are potentially very open to the ocean. However, the latter rim type 4 can also have *hoa* frequently closed by sand bars that run parallel to the lagoon.

Using a GIS software (QGIS 3.10.7), for each atoll, one single true color pan-sharpened multispectral very high spatial resolution (1 meter) IKONOS satellite image acquired after 2002 was used to identify by visual photo-interpretation the location of each *hoa*, and materialize their width with two linear segments parallel to the general perimeter of the atoll rim (Fig. 2). One segment corresponds to the lowest water level without water entrance (L_{min}) and the other should correspond to the highest level (L_{max}). The latter would correspond to level of water reached during high tides and high wave events, up to 4 meters, hence still below cyclonic levels. Cyclones are extremely rare in Tuamotu, and are not considered here (Laurent and Varney 2014). In all *hoa* morphologies, the limit of the intertidal area that would mark these two levels are visible due to a change in color, from brown to grey or white (Fig. 2). The water level in the *hoa* at the time of the image acquisition is not a reliable criteria because it only shows the conditions at the time of the image, not the upper or lower limit conditions. The brown area corresponds to surface colonized by cyanobacteria, and thus regularly under water, while areas permanently dry remain grey or white. In the case where soft borders and sand banks are present, their outer limit would mark the position of aperture L_{min}, but they were always considered as totally submerged in high swell conditions. These image-based clues for the interpretation of important atoll landscape parameters including aperture are fairly robust to changes in image resolution and qualities (Andréfouët et al. 2003). Considering the width and shape of *hoa*, using 1 meter resolution data means that the error in length of a segment is far less than a maximum 10% of the actual value if it was measured on site. While the accuracy of the segment length estimate is high using 1-m resolution images, where to put this segment can be problematic in some cases in particular for the rim type 4. Indeed, they often displayed complex sand banks and intertidal structures that mark where the flows occur (Fig. 2), and in some cases flows are not necessarily directed from the crest directly towards the lagoon. Identifying the efficient sections in terms of transport are thus not always straightforward in this case.

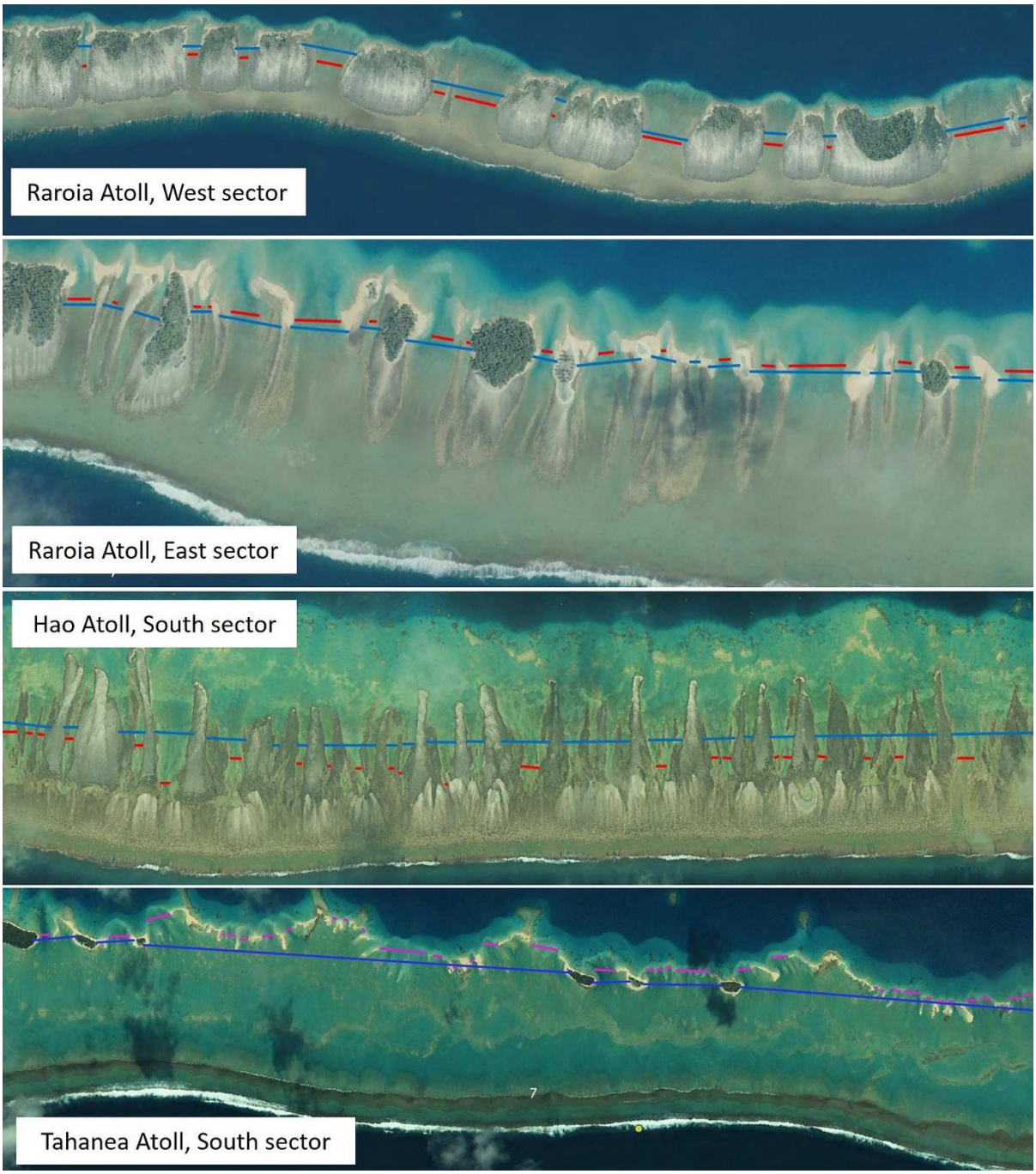

Figure 2: Examples of atoll rims and hoa *(rotated to have the ocean at the bottom and the lagoon on top of each image). Sectors from top to bottom are 4.5, 2.5, 3 and 6.5 km long respectively, with illustration of the locations where water can effectively enter the lagoon through the L_{min} (red or purple)* and L_{max} *(blue) segments during the lowest and highest wave conditions respectively. From top to bottom, the examples illustrate configurations with small to high differences between L_{min}* and $L_{max.}$ *The Tahanea sector at the bottom is an example of rim type 4, with L_{min} positioned between sand banks, while L_{max} is positioned straight between the few islets (visible as ellipsoidal forms).*

Further, a depth (Z_{min} and Z_{max}) was also assigned to each L_{min} and L_{max} linear segments. This depth is also not inferred by the water level that would be valid only at the time of image acquisition but was

informed based on general knowledge on *hoa* morphology described in numerous monographs, and ranged between 20 cm till 2 meter maximum (e;g., Newell 1956, Chevalier 1969, Battistini et al. 1975, Delesalle et al. 1985). This knowledge also comes from hundreds of *hoa* visited in the past thirty years in the course of various Tuamotu atoll projects (S.A. unpublished data). Overall, the use of Z_{min}, Z_{max},, L_{min} and L_{max} provide a way to characterize the variability of the flows at rim and atoll scales, bounded by a minimum and a maximum flow value, in the case of no other *in situ* hydrodynamic measurements exist.

The azimuth angles θ of all L_{min} and L_{max} segments were computed to provide their orientation relative to the direction of incoming swells (see below). In addition, each linear segment was assigned to a rim sector (as in Andréfouët et al; 2001a). A rim sector is characterized by a single direction, exposition, barycenter, and type of morphology.

Wave data

The wave data used in this study are similar to that of Dutheil et al. (2021) but also includes the year 2019. Briefly, a multigrid two-way nested configuration of the WAVEWATCH III (hereafter WW3; Tolman, 2009) spectral model version 6.07 (https://polar.ncep.noaa.gov/waves/wavewatch/) was used to provide, at 0.05° resolution around the atolls of interest, the peak direction (Dp), the peak frequency (Fp), and the significant wave height (Hs) every three hours from 2000 to 2019.

Because the propagation of waves is impacted by atolls, the obstruction scheme of Chawla and Tolman (2008) was used in the simulations. In practice, the energy is locally attenuated in areas where atolls should impact, or block the incident energy. However, the obstruction scheme is based on a global bathymetry (GEBCO 30″ bathymetry 2014 version: http://www.gebco.net/data_and_products/gridded_bathymetry_data/), which happens to be inaccurate in several areas within the Tuamotu. We therefore did not blindly use the closest outer oceanic WW3 grid point to assign wave data to a rim sector, but we manually assigned to each rim sector a valid WW3 grid point to avoid incorrectly obstructed signals (Fig. 3).

For each rim sector, from the assigned WW3 point, were extracted Hs, Tp and Dp at each 3h output. We also extracted for each WW3 point the maximum and minimum Hs for the entire period, respectively Hs_{max} and $Hs_{min.}$ We considered that water levels corresponding to L_{max} and L_{min} were reached during the conditions represented by Hs_{max} and $Hs_{min..}$

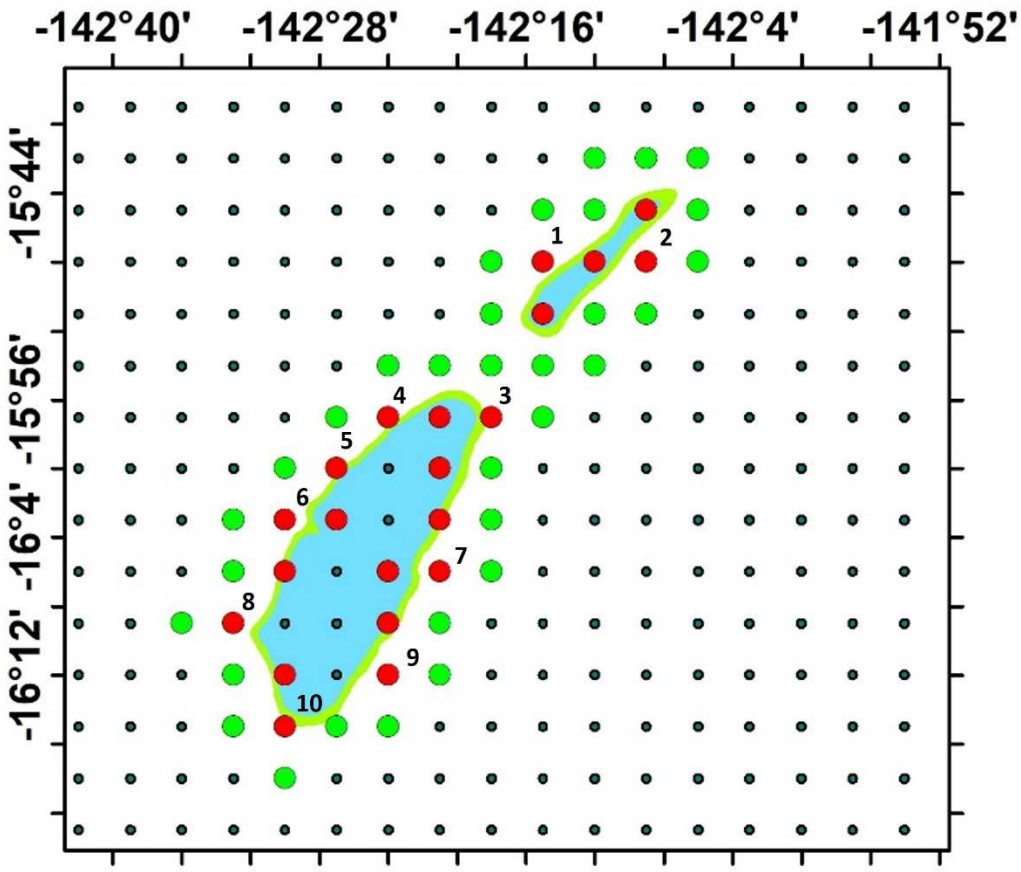

Figure 3: Example of the WW3 grid (small black dots) and obstructed cells (red dots) around Raroia and Takume, two pearl farming atolls in Tuamotu Archipelago. Because of inaccurately located obstructions, an automatic reading of wave data (e.g., using the closest WW3 node from the barycenter of a rim sector) cannot be performed. For instance cells 1-10 are not adequate because they are obstructed and outside the atoll. Instead, wave data are read from manually selected unobstructed cells close to the rim and outside the atoll. Green dots show these cells deemed valid for further analysis.

Estimates of water flows through the atoll rims

For each rim sector, each linear segment within that sector is assigned to the same WW3 grid point as selected above. (Fig. 3) Then, at each 3h output, a hydrodynamically effective section was computed following:

$$S = \left(\frac{Lmax - Lmin}{\mathrm{Hs_{max}} - \mathrm{Hs_{min}}}(Hs - \mathrm{Hs_{min}}) + Lmin\right) \times \left(\frac{Zmax - Zmin}{\mathrm{Hs_{max}} - \mathrm{Hs_{min}}}(Hs - \mathrm{Hs_{min}}) + Zmin\right) \quad \text{(Equation 1)}$$

This equation stipulates that the effective transport of water through the rim sector varies with time according to a vertical section *S,* which depends on wave height *Hs*, which itself potentially modifies the width and depth of each of the *hoa* on this rim sector, within its L_{max}-L_{min} and Z_{max}-Z_{min} ranges that are achieved between the Hs_{max} and Hs_{min} conditions. The values at each 3h model output are averaged to provide a daily estimate.

To estimate the daily averaged wave-driven flow through each relevant *hoa* sections of each rim and for each atoll, we used the generic relation for daily flow established by Aucan et al. (2021), with:

$$U = \mathrm{A} \times Hb + \mathrm{C} \quad \text{(Equation 2)}$$

U is the water speed (m.s^{-1}) in the *hoa*, Hb is the equivalent breaking wave height given by:

$$Hb = \mathrm{Hs}^{4/5} \times \mathrm{Tp}^{2/5} * \sin(\mathrm{Dp} - \theta) \quad \text{(Equation 3)}$$

With Hs the significant wave height, Tp the peak period and Dp the peak direction, respectively. A and C are constant values related to the effects of waves on the reef, and ocean and lagoon water level differences, and were set to A = 0,113 and C = -0,151 in Aucan et al. (2021) based on the average of all Raroia atoll measurements. However, we note that A and C can vary by *hoa* and by type of rim for a best local adjustment (Aucan et al. 2021).

In each *hoa*, the daily wave-driven flow *F* (in m^3.d^{-1}) is computed as:

$$F = U \, x \, S \quad \text{(Equation 4)}$$

The total daily flow for an atoll (F_{atoll}) is finally computed with the sum of *F* across all *hoa* along the atoll rim.

Lagoon and sub-lagoon water renewal times

The water renewal time *Tr*, in days, as it was estimated in Andréfouët et al. (2001a) is a lagoon-scale timescale indicator (Lucas and Deleersnijder 2020) computed as the ratio between the lagoon volume and daily wave-driven water inflow F_{atoll}.

$$Tr = \frac{Volume_{atoll}}{F_{atoll}} \quad \text{(Equation 5)}$$

Previously, the lagoon volume for each atoll has been estimated based on statistical morphometric relationships (Pagès and Andréfouët 2001, Purdy and Winterer 2001), in particular by relating the surface area and the volume, with a log relationship. However, atolls that do not fit the relationship can be easily shown (as discussed in Andréfouët et al. 2020). Therefore, we computed the renewal times only for atolls for which a precise measurement of the volume was available, namely Raroia, Takapoto, Ahe, Takaroa, Mopelia, Takume (Andréfouët et al 2020), and Moruroa (Tartinville et al. 1997) (Table 1).

For other atolls with unknown volume, a sub-volumic lagoon water renewal time *Tr_s* , in days, was computed as the ratio of daily water inflows to the volume of an arbitrary layer of lagoon water. We considered here the 1-meter surface layer. This volume can be accurately estimated since the surface

area of each lagoon was precisely measured using remote sensing satellite images (Andréfouët et al. 2005).

$$Tr\_s = \frac{Surface_{atoll}}{F_{atoll}} \quad \text{(Equation 6)}$$

If there is zero total inflow F_{atoll}, then Tr and Tr_s are theoretically infinite.

Spectral decomposition of wave-driven flows and water renewal times using wavelet transforms

Using the 2000-2019 WW3 data time series, it is thus now possible to compute for each atoll:

- time-series of daily inflow F per hoa assuming a linear response of aperture to swell (L_{min}-L_{max}),
- time-series of daily inflow F_{atoll} for the entire atoll,
- time series of renewal time Tr_s based on F_{atoll} and the surface of the lagoon.

For the lagoons with known volume, we can compute:

- time series of renewal time Tr based on F_{atoll} and the volume of the lagoon.

The time series are analyzed with a wavelet decomposition to estimate both the frequency, and duration of each spectral component. A very detailed explanation of the use of wavelet decompositions is available in Torrence and Compo (1998). This decomposition can be seen as an extension of the classical Fourier decomposition, where a time series is projected on a base of functions (sines and cosines). Wavelet decomposition uses the same mathematical formalism, but the base of functions is made of elementary functions that are explicitly localized both in time and frequency. Each wavelet $\psi_{s,t_0}(t)$ is built from a "mother" function $\Psi_0(t)$ following:

$$\psi_{s,t_0}(t) = f(s,t_0) * \Psi_0\left(\frac{(t-t0)}{s}\right) \quad \text{(Equation 7)}$$

Where s is the wavelet scale and t_0 the wavelet translation and $f(s,t_0)$ is a normalization factor, used to ensure the conservation of energy along all scales (more details on the proper definition of this factor can be found in Liu et al 2007). By varying the scale and translating along the time index, one can generate a wavelet for a given time and duration. The mother wavelet was chosen as the classical Morlet wavelet as it efficiently describes both the temporal and frequency components of a signal (Labat 2005). This wavelet consists in a plain wave modulated by a Gaussian. The components of this wavelet are represented on Figure SM1. Confidence levels of 95% were computed by comparing the analyzed signal to a red-noise process with a lag-1 coefficient calculated from the data set, following Torrence and Compo (1998).

Time integrated renewal-time

The previously defined renewal times, *Tr* and *Tr_s,* are derived daily from the corresponding flow at that time. They do no account for the succession and history of events, while there are many evidences that hydrobiological processes in a lagoon water column takes time to develop under the influence of processes that can occur in few hours to weeks (Delesalle and Sournia 1992). This can be better assessed with the concept of lagoon water age. Following Deleersnijder et al. (2001), the age of a particle of seawater is defined by the time elapsed since it entered the area of interest (Lucas and Deleersnijder 2020). Here, because very limited data is available, the computation is based on simple assumptions. Specifically, only two positions are possible for water particles: either inside or outside of the atoll. If they are outside the atoll, their age is prescribed to be zero. If they come inside the atoll, their age grows over time. The atoll volume is assumed to be constant during all the simulation, so every water particle that enters the atoll pushes a water particle outside of the atoll and the only possible way for a particle to leave the atoll is through the action of *hoa* inflows that we have computed. This provides a new time-dependent metric, that takes into account the history of the renewal times across a period of time, hence we named this metric 'time integrated renewal-time', or *Tag*(t). It is defined as the mass-weighted, arithmetic average of the ages of the considered particles:

$$Tag(t) = \frac{\sum_i a_i m_i}{\sum_i m_i} \qquad \text{(Equation 8)}$$

Where $a_i$is the age of the particle i, and m_i is its mass. Here the computation is very simplified as there are only 2 kind of particles:

1. New particles entering the atoll from the *hoa*. Their age is 0, and their mass is equal to ρV_{hoa}, where ρ is the density of sea water, and V_{hoa} the volume of water entering the atoll through the hoa. We computed the *Tag* on a daily time step, so $V_{hoa} = F$.

2. Old particles, which were inside the atoll the previous day. Their age is not null and grows over time. Their mass is equal to $\rho(V_{atoll} - V_{hoa})$, where V_{atoll} is the volume of the atoll. Hence, *Tag(t)* can be defined as

$$Tag(t) = (Tag(t - dt) + dt) * ((V\_atoll\ - V\_hoa)/V\_atoll\ ) \qquad \text{(Equation 9)}$$

In our case, on a daily time step, dt=1 day so the age of the old particles is equal to Tag(t - 1)+1, and equation 9 can be rewritten as:

$$Tag(t) = \ (Tag(t - 1) + 1) * \left(1 - {}^{1}/_{Tr(t)}\right) \quad \text{(Equation 10)}$$

Validation

The computations presented above are based on numerous proxies, either geomorphological or hydrodynamical. Atoll-scale F_{atoll}, *Tr* and *Tr_s* are difficult to validate using field data, but it is nevertheless possible to quantitatively evaluate the accuracy of *F* by comparing time series of water velocities in selected *hoa* with results issued after Equation 4. Specifically, in the past, two atolls have

been instrumented in several legs and for different *hoa*: Ahe from June 2008 to September 2009 (Dumas et al. 2012), and Raroia from May 2018 till March 2019 (Aucan et al. 2021). We compared measured velocities versus modeled velocities (using WW3 wave data and Equation 4) for these sites and periods.

Results

Modelling wave-driven water flows through hoa

The Figure 4 compares for different hoa in Ahe and Raroia atolls the velocities modeled using WW3 data and Equation 4, and the measured velocities. The velocities are in agreement and follow the same variations overall (r^2, the determination coefficient of the linear regression between measurement and model is between 0.52 and 0.68) although the modelled velocities are generally overestimated. The Nash-Sutcliff Efficiency (NSE) coefficient reflects better the differences between the time series. A negative NSE reflects that the variance of the modelled data is larger than the variance of the *in situ* reference data. NSE=0 means that variances are equal. The lowest performance (NSE=-2.31) is achieved for Raroia's H3, which corresponds to the Rim type 4, while the other sites perform much better (Figure 4). We also note that with Equation 4, negative, or null, modeled flows can occur even for positive wave height.

Several factors, of different nature, can explain these negative values. First, given the large size of the WW3 grid, the swell diffraction cannot be resolved exactly everywhere, so there may be instances of swell direction going away from the rim, and hence, a negative flow is computed. Numerically, this would be equivalent to the *hoa* pushing water from the lagoon out to the ocean. This mechanism is possible in reality (see Callaghan et al. 2006) when the lagoon level is higher than sea level, possibly due to wave flows entering the lagoon on the other side of the lagoon of the *hoa* at stake. But a negative flow on a rim directly generated by incident waves on that rim is not possible, and rather correspond to a null, or nearly null, flow. Second, even if the different 2D morphology of atoll rims are described in the nine aforementioned rim types, many additional 3D fine-scale morphological differences from one site to another were not included in this characterization (e.g., crest height at the wave impact zone, the slope of *hoa* across the rim, etc.). These differences can induce a different A and C in order to model precisely the flows with Equations 2-4. Tuning the coefficients A and especially C is a way to avoid negative flows when using WW3 data. However we lack measurements in most of these fine-scale configurations to refine precisely what could be the local coefficients A and C and assess their range of variations. Therefore, it was decided that C was set to zero for all rims and all atolls with the results that no negative flows due to incident waves could occur.

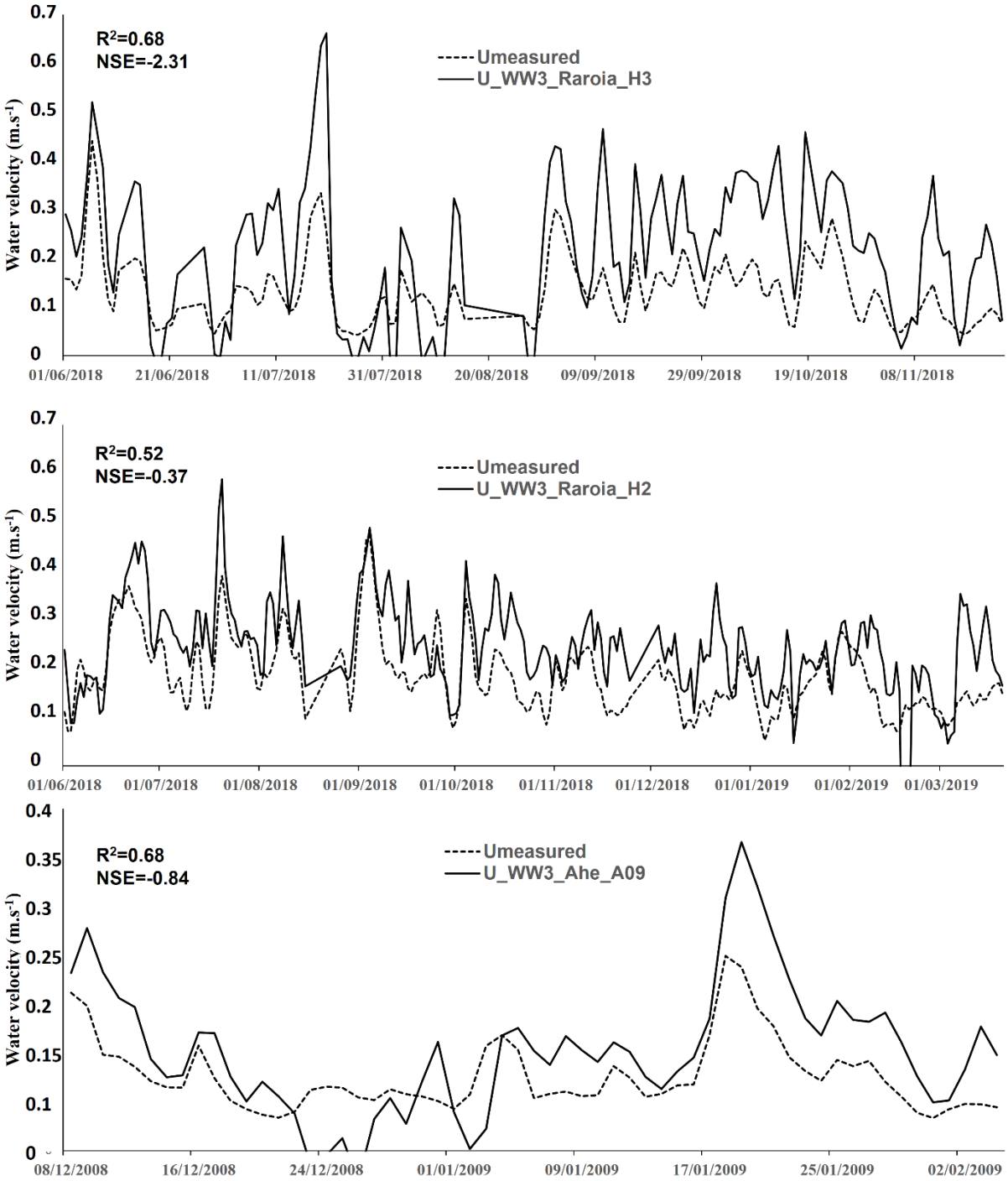

Figure 4: For three selected hoa: *measured versus modelled daily-scale water velocities U based on Equation 4 and WW3 data. Top and middle, two* hoa *from Raroia atoll from where the equation 4 has been calibrated using in situ wave height measurement (and not WW3 wave data like here, more details on calibration in Aucan et al. 2021). Bottom: comparison for one* hoa *in Ahe atoll (more details in Dumas et al. 2012) that has not been used for Equation 4 calibration. Determination coefficient of the linear regression between measurement and model are provided (R^2), as well as the Nash Sutcliff Efficiency coefficient (NSE).Negative modelled values are not shown.*

Aperture of atoll rims

The total aperture L_{min} and L_{max} per atoll are provided in Table 1. By dividing the perimeter for each atoll (Table 1) a minimum and maximum degree of aperture can be computed using respectively L_{min} and L_{max}. The percentage of aperture increase when shifting from L_{min} to L_{max} ($Ap\%$, Table 1) range from 135% to 2200%. Forty-three of the 74 atolls had an increase lower than 400%. Sixty-six atolls had an increase lower than 800%.

Time-series of wave-driven water flows and renewal times

Examples of time-series of water flows F_{atoll} (in $m^3.d^{-1}$) are provided in Figure 5 (top panels). For some atolls, spikes two or three orders of magnitude higher than the average flows occurred during 3 to 5 days. They can be explained by the few tropical cyclones that crossed the western part of the study area between 2000 and 2019, notably in February 2010 (cyclone Oli), or by the type of rare large swell events described in Andréfouët et al. (2012).

Examples of time-series of renewal time *Tr* and *Tr_s* are provided in Figures 6 and 7 (top panels). In this case, and for some very closed atolls with a only a few *hoa*, several spikes can be related to extremely long renewal time (several centuries), due to extremely low flows that are not visible immediately in the flow time series (as in Figure 5, top panel). Unlike inflows F_{atoll} for which very high values are generally preceded by a progressive increase during a couple of days, the *Tr* and *Tr_s* spikes are often reached for one day only without transitions and should be interpreted with caution.

Wavelet transforms of lagoon flows and water renewal times

Figures 5 to 7 are representative examples of wavelet transforms computed for *F*, *Tr_s* and *Tr* respectively. In Figures 5-7, the significant peaks on the spectrum curve can be interpreted in terms of intensity and periodicity of the signals. Peak periods can be different dependent on the metrics.

For the flows F_{atoll} (Figure 5), significant period values show a clear annual periodic pattern for all the three atolls shown. These atolls also represent how this annual signal can be interrupted and non-significant during some years depending on each atoll. Takaroa represents atolls with a weak annual periodicity. They also show slightly different significant periods below 16 days.

For *Tr_s* (Figure 6) the significant period can be different than for F_{atoll}. For instance Takaroa has almost no periodic significant signal across the spectrum, and only a very low peak at the annual time scale. It rather shows a stochastic behavior without any significant frequency. Conversely, both Raroia and Hikueru maintain a strong annual periodic pattern of renewal.

Tr and *Tr_s* differ by a constant specific to each atoll (i.e., its volume) and values are rising. Therefore, for *Tr* (Fig. 7) the signals for the 7 atolls with known volume have similar relative pattern than *Tr_s* (see for instance Raroia and Takaroa also shown in Figure 6), but the intensity of the wavelet contribution are different between *Tr* and *Tr_s*. In term of variation between years and their energy, Takapoto, the most closed atoll of the group in Figure 7, has the highest inter-annual differences in the scalogram in the 16-128 days periods, although these are non-significant. Conversely, Moruroa, the most open atoll of the group; very exposed to waves from all directions (the only atoll without any pearl farming record) has a strong annual periodic signal, well-marked on the scalogram at all years. For all the other atolls of the group, that all have a history of pearl farming and spat collecting, the annual signal is weaker and interrupted, sometimes for several continuous years.

Due to the range of values, the power spectra were all normalized following Smith et al. (1998) and overlaid on Figure 8 for visual comparison. With the normalization, significance is not known and differences between spectrum need to be evaluated based also on the significance of the initial peaks (see Figs. 5-6). Noteworthy is the variation of the ~360-day period signals between atolls (Fig. 8). The comparison of the wavelet transform graphs for all atolls suggests different processes occurring at different time scales. For instance, for the flows F_{atoll}, several atolls have a separate shoulder at around 24 days, or around 64 days (Fig. 8, top panel). Interestingly, these include all pearl farming and spat collecting atolls for which we could also compute *Tr*. For *Tr_s*, the spectra are the most widespread below the 4 days threshold. The same pearl farming and spat collecting atolls also have the lowest power value below 8 days and a larger shoulder at around 64 days. The individual behavior for the pearl farming and spat collecting atolls with a known volume can be seen on the F_{atoll}, *Tr_s*, and *Tr* spectra (Fig. 8). For *Tr*, the most open atolls during the minimum wave conditions (higher A_{min} for Moruroa and Mopelia) have the highest normalized power below the 8-day period, and the lowest at around 64 days compared to atolls with a more closed geomorphology. These seven atolls do not capture the peak at 290 days visible for many atolls on the *Tr_s* spectra.

Hereafter, in the discussion section, we interpret these figures 5-8 principally based on the most prominent signals that should be robust to all possible bias in the computations and proxies used here. Specifically, these are: 1) the significance of a power spectrum peak at around 360 days, which marks an annual periodicity (Fig. 5-8); 2) the differences between pearl farming, and non-pearl farming atolls, and in particular for the productive spat collecting atolls (Table 1) (Fig. 5-8).

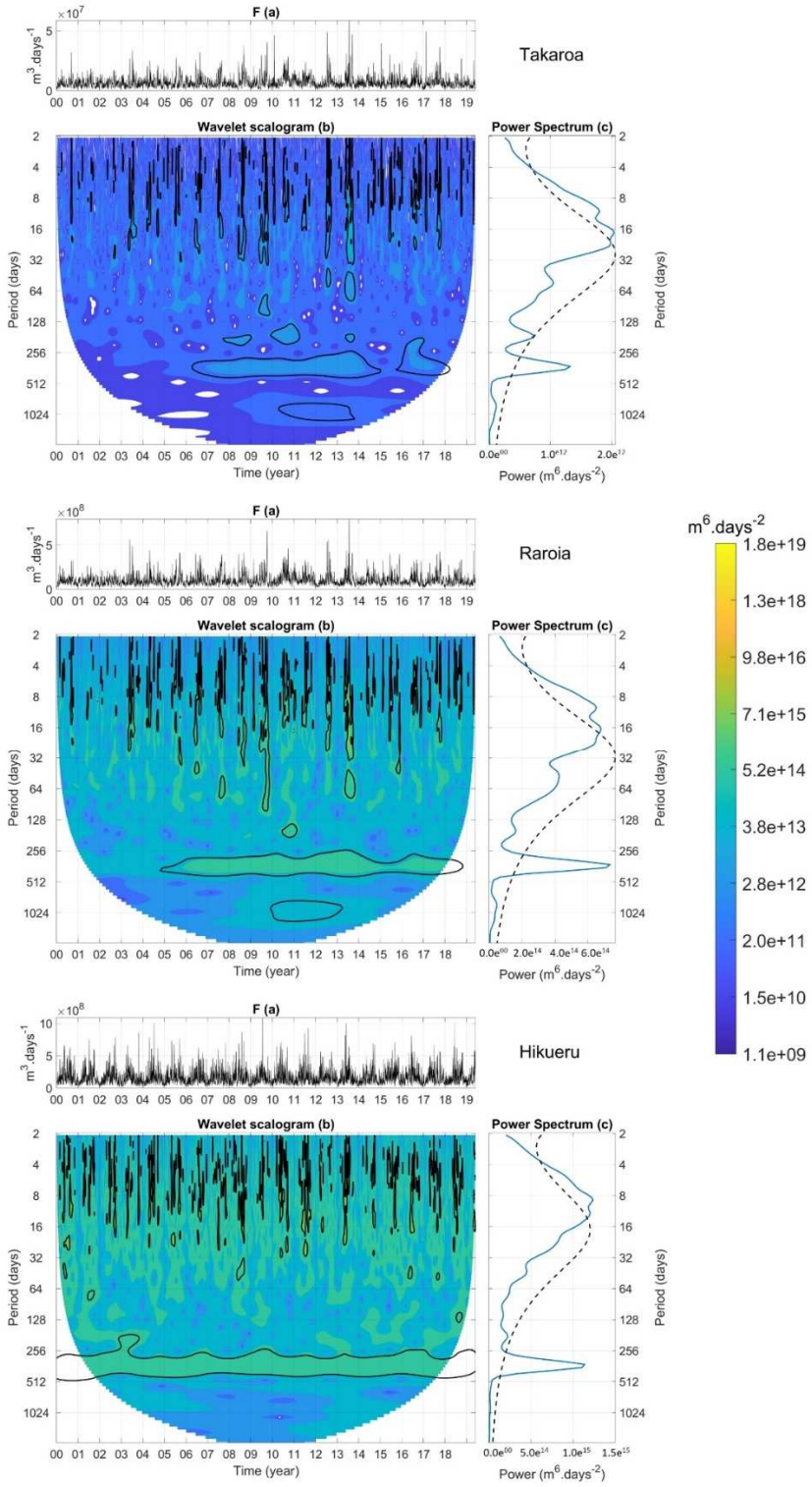

Figure 5: Panel A is the data time series. Panel B is the wavelet scalogram where the x-axis represent time (or years between 2000 and 2017), and the y-axis represent the wavelet periods in days. In other words, fast daily or weekly-events appear on the top of the scalogram, while longer periods are toward the bottom. The power (color bar) reflects the wavelet contribution to the overall signal. Scales for power are similar for each plot. Significant periods are highlighted by the black contour. The panel C is the power spectrum that integrates the results of Panel B along the time axis. The dash line is the statistical significance threshold. Values found above this line represents therefore the important time scales, and periodicities, such as the annual periodic component (peak centered between 256-512 days) as well as several higher frequency processes generally below the 16 day-threshold.

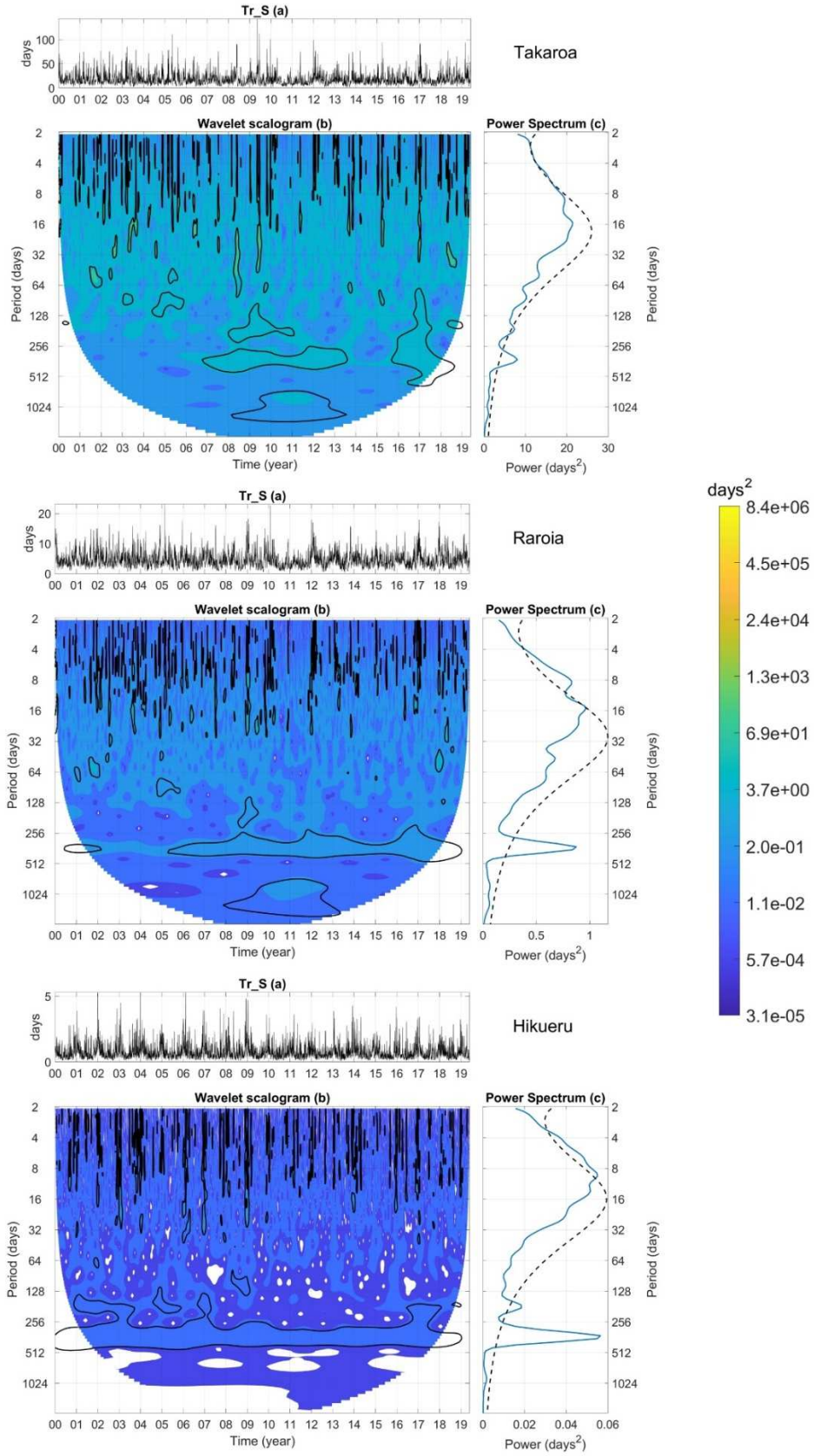

Figure 6: The different panels A, B and C are explained Figure 5. Examples of wavelet analysis of sub-volumic renewal rates Tr_s (in days) Here, Takaroa represent atolls without any clear annual periodicity, unlike its flows in Figure 5.

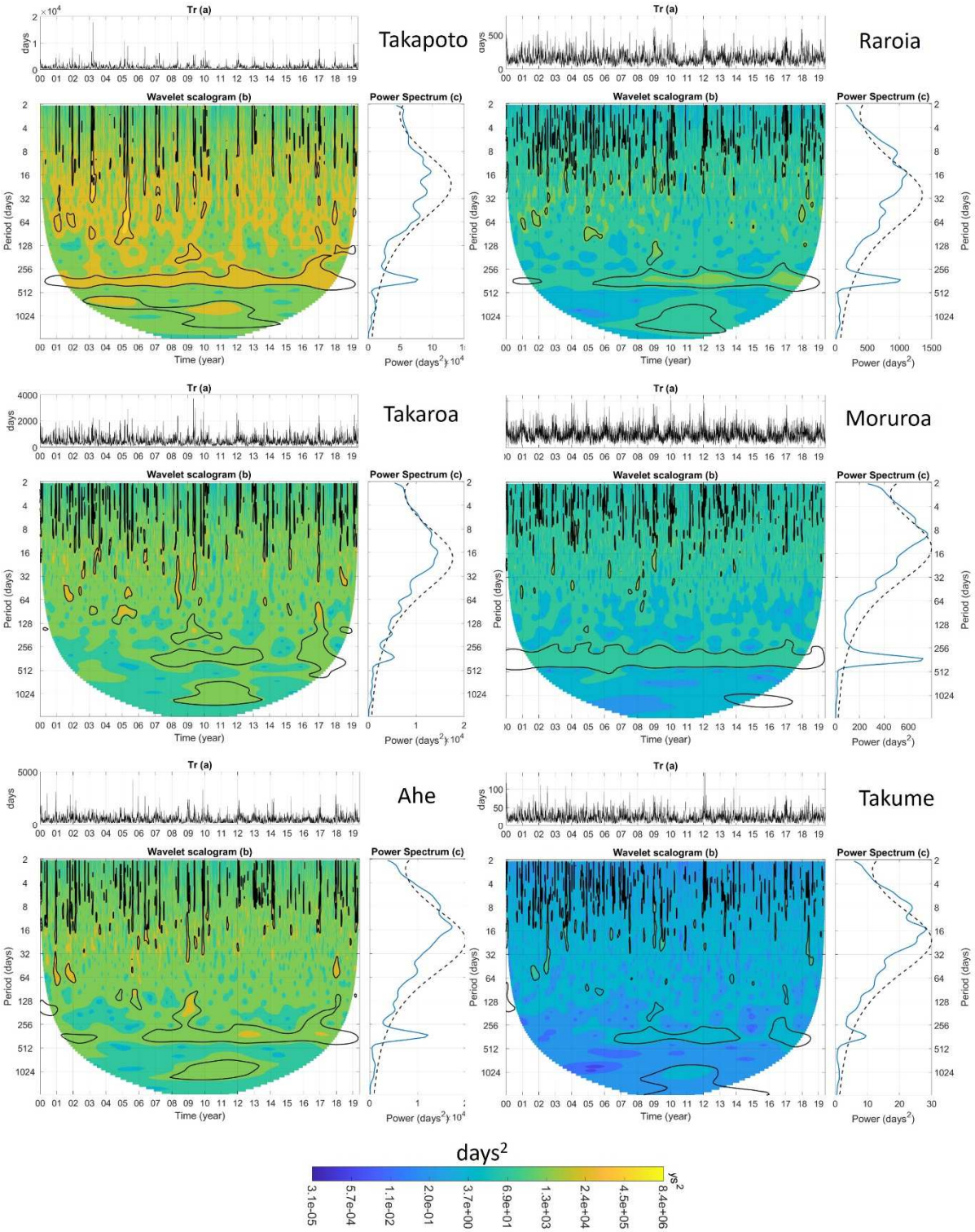

Figure 7: The different panels A, B and C are explained Figure 5. Wavelet analysis of renewal rates Tr (in days) for the atolls with known volume (Mopelia Atoll not shown). The power (color bar) reflects the wavelet contribution to the overall signal. Scales for power are similar for each plot. Atolls are ranked from left to right and from top to bottom, by decreasing average renewal time, or, in other words, by the overall intensity of the scalogram power, from yellow to dark blue dominance (see color bar).

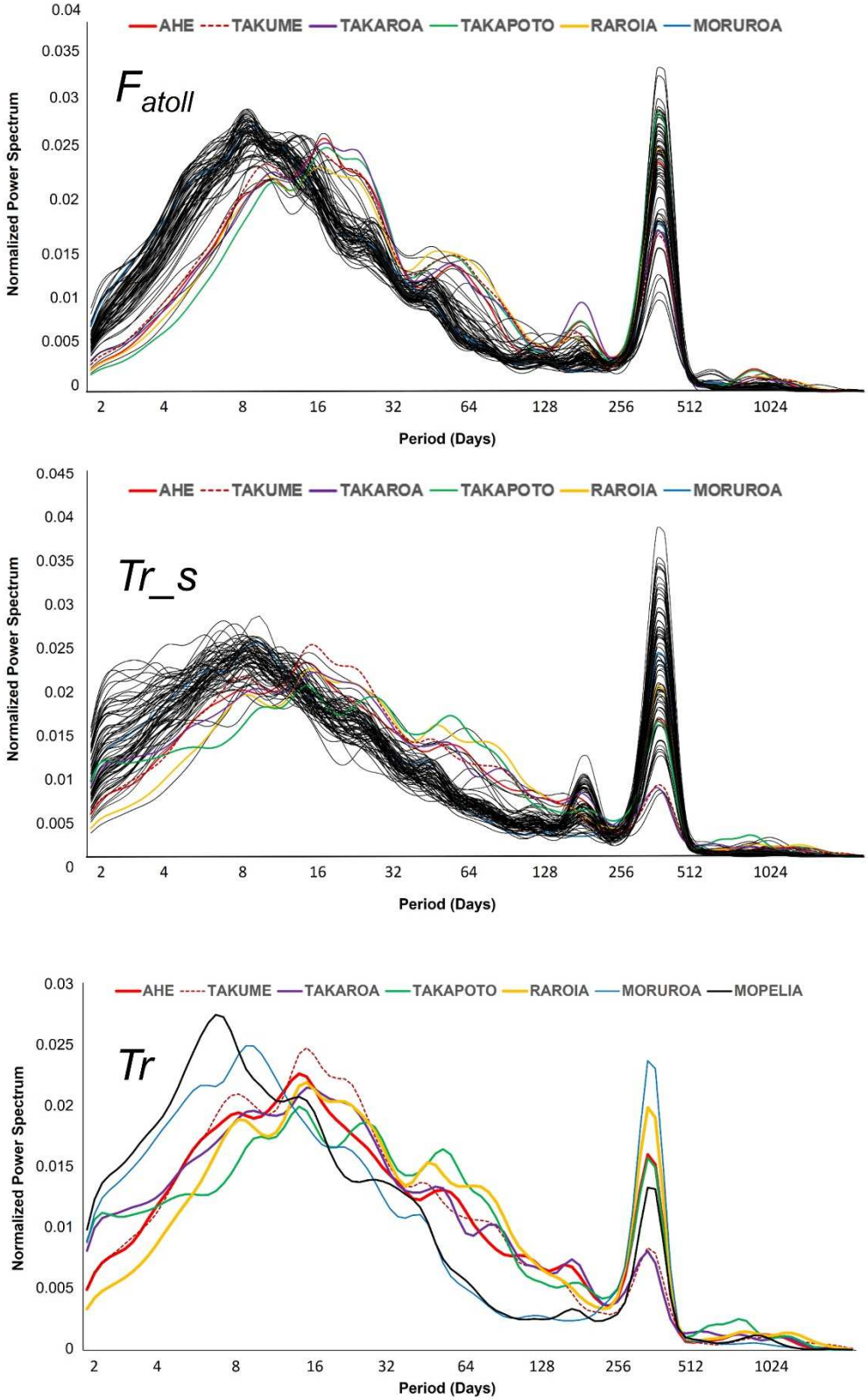

Figure 8: Top and middle panels: Overlay of unitless normalized power spectrum for all the 74 atolls for F_{atoll} (top panel) and Tr_s (middle). Lower panel: overlay of normalized power spectrum for Tr for the 7 atolls with known volumes. For F_{atoll} and Tr_s the pearl farming and spat collecting atolls (Ahe, Takaroa, Takapoto, Raroia, Takume) are outside the bulk of the other atolls, with a lower and a higher normalized spectra in the 2-16 day and 16-128 days periods respectively. For all metrics, the highest variability is for the annual peak period at ~360 days, visible here between 256-512 days. For

Tr, and keeping in mind the small number of atolls, highest variability also occur in the 4-8 day periods.

Time-integrated renewal time

The patterns of aging computed using equation 6 from *Tr* for the atolls with known volume are shown in Figure 9. Three groups are apparent. A first group including Ahe, Takaroa and Takapoto exhibits a periodic annual variation which is above 250 days, with Takapoto being higher than 400 days. These values are reached after 3 years of initialization time (or spin-up), which also reflects the slow average renewal. Inter-annual variations show differences between years, with irregular amplitudes, for instance between years 2011 and 2016. Raroia and Moruroa have a more regular periodic pattern in inter-annual variation, centered around 100-150 days, although Raroia shows similarities with the first group. These four atolls (Ahe, Takapoto, Takaroa and Raroia) also all display a decreasing trend in the first half of the time series, till year 2012, followed by an increasing aging trend. This is not seen in the other atolls. For Raroia and Moruroa, the spin-up is about one year before the annual oscillations can occur. Finally, Takume (and Mopelia, not shown) shows fast variations with an average of 15 days, hence one order of magnitude lower than group 2. In this case, the spin-up is very fast, in a matter of days.

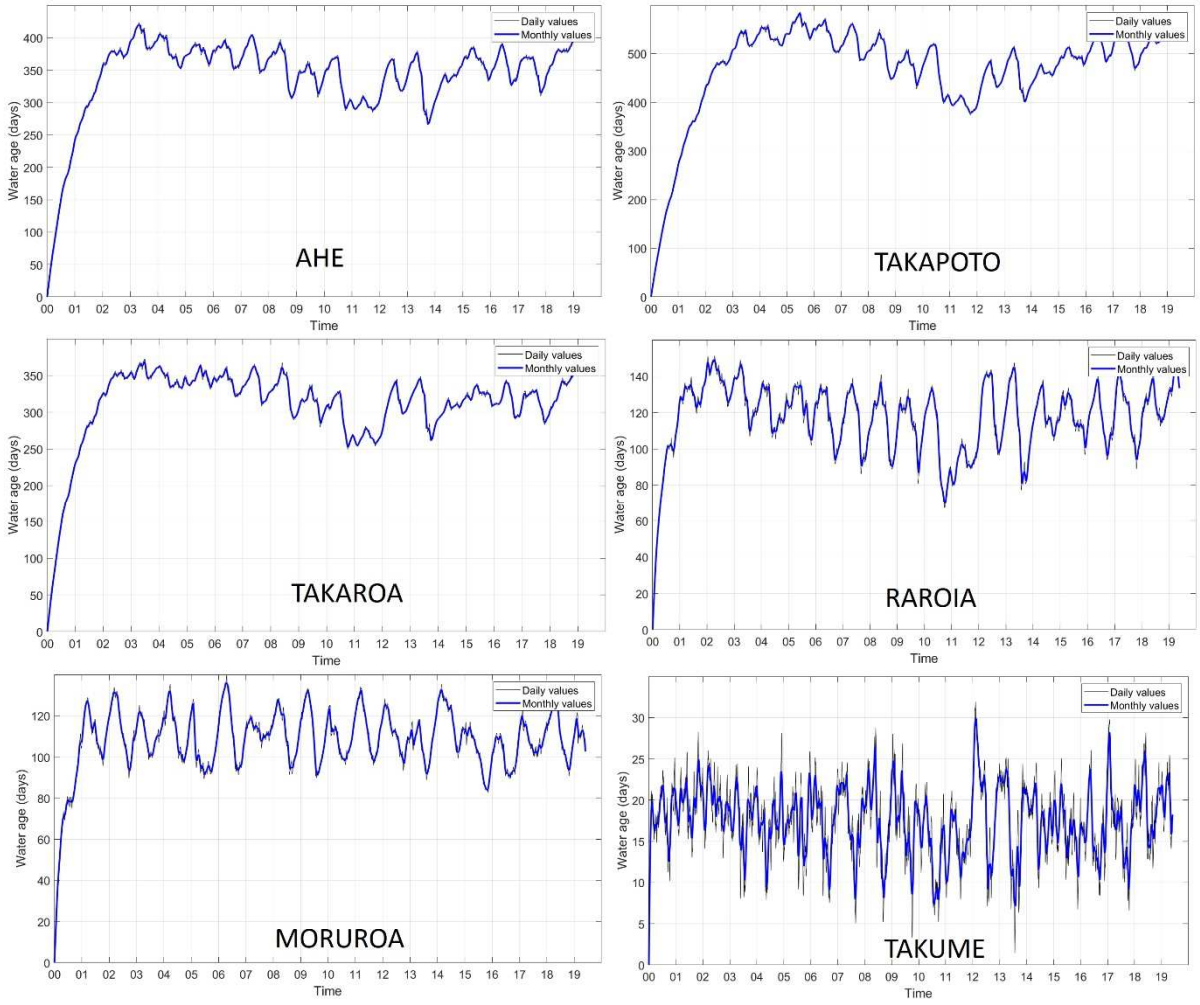

Figure 9: Time-series (2000-2017) of water aging (Tag) for six atolls highlighting three groups of average aging time scale. Ahe-Takapoto-Takaroa, all spat collecting atolls, above 250 days, Raroia and Moruroa at around 100-150 days on average, and Takume around 15 days on average.

DISCUSSION

Potential of different wave-driven renewal time metrics

The results presented here describe the wave-driven water renewal of atolls based on 1, 2, and 3 dimensions metrics which are: F_{atoll}, the wave-driven flow through *hoa* (1D); *Tr-s,* the renewal time computed over the lagoon surface layer (2D); and *Tr* for the entire lagoon volume (3D). These metrics were computed from a 20-year time series of wave simulated data at high resolution (0.05°) in the area of interest, and from a geometric characterization of the *hoa* aperture in the atoll rims based on very high spatial resolution (1 meter) satellite imagery. A total of 74 French Polynesia atolls are processed, spanning roughly a 2300 by 1200 km region. The hypotheses and data sets allowed estimating the periodicity of wave-driven water renewal of atolls despite their high morphological diversity and geography.

The entire set of metrics (Figs. 8-9) is a rich database from which we primarily focus on the behavior of selected pearl farming atolls. Further work could investigate the statistical differences between significant periods among all atolls for each metrics, or by including all metrics, but the different patterns visible for selected atolls can also be used to highlight unambiguous end-members. The transition between atoll-types probably forms a continuum (considering Fig. 8) and, cautiously, we suggest that it would be first necessary to refine some of the intermediate processing steps, including local field work, before providing a final classification of atoll. These refinements are discussed hereafter in the Perspective section.

In the context of the hydrodynamic functioning of atolls, our strongest hypothesis was to focus only on wave-driven flows across shallow *hoa* to characterize the differences between atolls, neglecting the other tide-driven processes, and the passage of water through deep passes when they exist. Therefore, we explicitly set ourselves in a non-holistic, atomistic, characterization of water renewal processes *sensu* Lucas and Deleersnijder (2020). In other words, we do not claim to provide an analytical characterization of the hydrodynamic functioning of atoll lagoons as it can be provided by numerical models (Kraines et al. 1999, Tartinville et al. 1997, Andréfouët et al. 2006, Dumas et al. 2012, Lindhart et al. 2021, Le Gendre et al. in prep.), but a relative characterization useful to rank and compare atolls, especially the pearl farming ones, in order to appreciate how unique these atolls might be in term of renewal processes during a 20 year period.

The different computed metrics have different assets and weaknesses. The water velocities can be compared with measurements (Fig. 4), and were summed over all *hoa* to give F_{atoll}, the total inflow per atoll, but they should require a normalization by atoll volumes or surfaces to allow the comparison between atolls, hence the use of *Tr* and *Tr_s*. Nevertheless, even without normalization, the spectral wavelet analysis is able to provide a timescale characterization of the wave-driven flows (Fig. 5). The compilation Figure 8 summarizes the diversity of the atolls related to wave's influx, and unfolds which temporal scales affect which atolls (Fig. 8). In particular, we found highly relevant a first dichotomy based on atolls with a strong annual signal which can be related to seasonal variations and regimes, and the others that seem affected by much more stochastic processes, of lower duration and time scales. This dichotomy was not described to our knowledge before. Further, we found that different atolls are affected differently by the high frequencies, with higher variations below ~32 days (Fig. 8), whether or not the annual pattern is strong. Finally, the wavelet analysis (Fig. 5) also points to peculiar years for individual atolls, and with renewal processes spread across different temporal scales across different years. It is unclear which processes have generated these peculiar years. The investigation of the reasons explaining these variations is behind the scope of this first analysis of the periodicity of lagoon renewal processes, but it clearly warrants further investigations, for instance by trying to link the atoll-scale processes with the variations of larger regional regimes and swell origins (Dutheil et al.

2021), and their anomalies (Andréfouët et al 2015). However, refinements are also required first (see below).

The wavelet analysis of *Tr_s* needs more precaution. Sub-volumic *Tr_s* normalizes the total flows by an arbitrary volume which is the upper 1-meter deep layer of the lagoon. Flows F_{atoll} and sub-volumic renewal times *Tr_s* are temporally in opposition, and their asynchronous highest values could constitute a combined signature of atoll hydrodynamic forcing and functioning. Unlike flows for which a spike represents high values, spikes in *Tr_s* are congruent with flows almost null. As seen early in the process (see Methods), these spikes were often very short, one day only, and have little physical meaning. The wavelet analyses of *Tr_s* can be strongly biased by these spikes. Atolls with very limited aperture, or with only few *hoa* on only one side of an atoll are prone to these spikes. Therefore, atolls with limited aperture (Table 1), could be very sensitive to inaccuracies coming in particular from the wave data and from the equation 4 relating wave height with flow velocities (see discussion below). Setting the *C* constant equal to 0 resulted in adding a constant to the flow time series. As we are analyzing the variability of the flow, the influence of adding such a constant is negligible on the time-scale of the flow variations. It is however important on the renewal times, as this added constant modifies the maximum value that the renewal time can get. On the other hand, it removed extreme values of renewal times that had no physical sense and had very high influence on the scalograms (data not shown).

We suggest that to explain processes such as mass mortalities or phytoplanktonic blooms, the characterization of the successions between periods of low and very high renewal times could be too sensitive to the suite of proxies that we have used here. Yet, in the case of well flushed, well open, atolls without spikes, the differences between atolls are less prone to biases, and the interpretation of periodicities and events during peculiar year should be informative. Indeed, a strong disruption of wave-driven inflows, and period of water quality risks congruent with a high *Tr_s* could be visible as an unusual year in the wavelet scalograms. The figure 9 suggests for some atolls a decreasing aging trend across the years, followed by an increasing trend (e.g., Ahe, Takapoto, Takaroa). This can be related to slight change in the seasonality of wave regimes for geomorphologically closed atolls. Same conclusions arise for *Tr*. *Tr* provides a true renewal time by using the actual volume of the lagoon. Time scales are therefore much slower than for *Tr_s* (Figs. 6 and 7), but the caveats in using *Tr* are qualitatively the same as for *Tr_s*.

The lagoon water age variable, *Tag,* (Fig. 9) integrates the temporal dynamics, and could be for that reason more suitable for a direct comparison with other metrics of renewal computed with holistic 3D numerical models that also includes tide-driven processes, as well as wind-driven processes. The 3D

hydrodynamic models can provide a number of water renewal metrics (i.e., residence time, water renewal time, turnover time, e-flushing time) that have all specific definitions (Tartinville et al. 1997, Jouon et al. 2006, Dumas et al. 2012, Lucas and Deleersnijder 2020). Considering these inherent differences, one need to be cautious when comparing different metrics computed for different conditions and hypotheses. Similar to discussion in previous studies (Tartinville et al. 1997, Dumas et al. 2012), checking the agreement between metrics can be informative and point to necessary improvements, and complementarities between the schemes presented here. For instance, *Tag* shows three groups of atolls with contrasting range of values in term of aging waters. For Ahe atoll, from January to April 2009 and also in climatological conditions (constant tradewind forcing), it was reported an average e-flushing time of 80 days, with a largest value around 140 days. The renewal time was 252 days (Dumas et al. 2012). Here, for the same period of early 2009, T*ag* is around 300 days which is actually fairly consistent with the 3D-modeled metrics (Fig. 9). For Moruroa atoll, the values are also in agreement. Moruroa was modeled by Tartinville et al. (1997) according to different types of forcing, including a simulation called TWH (for Tide, Wind and *Hoa* inflows). The Moruroa H (*hoa*) factor is relevant to the present study. The turnover time was 128 days while our mean *Tag* estimate is about 110 days (Fig. 9). For this atoll, Tartinvillle et al, (1997) also discussed that vertical variation of the residence time is small compared with the turnover time, which emphasizes the inherent variation between each metrics. They further comment that including the *hoa* flows did not decrease the turnover time, as it would be the case in our study. Instead, the additional fluxes brought by wave-driven *hoa* inflows was flushed very rapidly through the pass, and that flux increased the strength of horizontal gyres that trapped their water particles inside the atoll, hence increasing the turnover time. In addition, we remind that Moruroa has the widest pass in the Tuamotu-Gambier atolls, and the behavior of reinforcing horizontal circulation gyres can be exacerbated by this unique feature.

Relevance for pearl farming atolls and spat collecting

A critical time-scale for pearl farming atolls would be the renewal time relative to *Pinctada margaritifera* pelagic larval duration, which is considered to vary between 20 and 30 days in the usual conditions of French Polynesia atoll lagoons (Sangare et al. 2019). Practically, for atolls with a pass like Ahe or Takaroa, spat collectors are not deployed near passes where flows are tide-driven (Dumas et al. 2012), and the questions of spat collecting potential in relation to *Tr_s, Tr,* or *Tag*, despite their non-holistic nature, are therefore justified and worthy of discussion. The time during which larvae are 'trapped' in an atoll lagoon is critical for the efficiency of spat collecting, the activity that form the basis of the entire pearl production process. Simply said, the longer the renewal time, the higher the potential for spat collecting should be, assuming that oysters effectively spawn in that lagoon, and that

temperature and planktonic food are adequate for pearl oyster larval survival (Thomas et al. 2016, Sangare et al. 2019).

As discussed above for Ahe, an interesting information provided by the wavelet scalograms, is the identification of shifting periodicities. For instance, a weak annual periodicity can be related to the absence of the signal around 360 days for few years, or , conversely the occurrence of a strong annual signal otherwise usually absent. Similar statements can be made for all periods. These may highlight inter-annual specific, unusual conditions during which an atoll could have experienced better than usual, or worst, farming/collecting results.

For the atolls for which the atoll volume is known, and for which *Tr* (Fig. 8) or Tag (Fig. 9) could be computed, three atolls are historically known for their spat collecting efficiency: Ahe, Takaroa and Takapoto, although this efficiency has been highly variable in the past decades. They form the group with the highest average Tag (>250 days). Raroia and Takume with lower Tag average value are also pearl farming atolls, with collecting activity, but have never been massive spat producers to the point of exporting spats to other atolls like the three others. The potential for spat collecting of Moruroa and Mopelia (not shown) are unknown because this activity was not tried or documented in these lagoons. When looking at the *Tr_s* scalograms and the amplitude of peaks in the spectra for the historically productive spat collecting atolls (Ahe, Apataki, Katiu, Manihi, Marutea Sud, Takapoto and Takaroa), it is however difficult to identify a clear criteria that would discriminate all these seven atolls from the rest of the 67 atolls.

Unfortunately, farmers do not provide, or even record, their spat collecting results even today after 30 years or more of practice. At best, it is known that a given atoll has been much more (or much less) productive than before, but without precise numbers. Documented spat collecting statistics would be tremendously useful to relate environmental conditions and periodicities of lagoon renewal with farming performances, but this remains unavailable. Therefore, it is difficult to discuss quantitatively some temporally-well defined episodes of spat collection in relationships with flows and renewal time.

Future research directions for Central Pacific Ocean atolls

The approach followed here, focusing on lagoon wave-driven renewal processes aimed to investigate, with spectral decomposition of three renewal metrics, and one aging metric, if groups of atolls can be identified and if these groups can be relevant in the context of pearl farming activity, in particular spat collecting potential. The work performed for the Tuamotu-Gambier here remain largely exploratory but should initiate further work on atoll functioning comparison and their typology. It is useful to

identify different lagoon behaviors, and future priorities and refinements. This work provides a unique large database that will be useful for further studies at different scales and continue developing a quantitative functional typology of atolls, that will be much more interesting than the previous typologies based on geomorphology only, with the number of passes (Salvat 1985), or the degree of aperture (Andréfouët et al. 2001a,b).

First, we suggest that the wavelet analysis is useful to understand with consistent parameters how atolls differ and this tool could be used with other forcing factors (wind, temperature, etc.). Here, wavelets provided a time-integrated signature of renewal rates. This is coherent with other developments in environmental sciences and oceanography. It is a very versatile tool, with numerous applications in hydrology (Onderka and Chudoba 2018, Desclaux et al. 2018). It is increasingly used for marine environmental and in particular environmental forcing characterization. In a coral reef context, early on, the water velocities on Ningaloo (Western Australia) reef flats due to breaking waves were analyzed by Massel (2001). Following applications looked at current and flows variations on Gulf of Mexico deep reefs (Teague et al. 2014, Valle-Levinson et al. 2020), as well as ENSO variations on the Great Barrier reef during the Holocene (Leonard et al. 2016), or reef topographical complexity (Duvall et al; 2019). Here, for the first time to our knowledge, it is applied to atoll lagoons, to follow the idea of characterizing these lagoons through the spectral analysis of their renewal time (Andréfouët et al. 2001b). It is likely that more work will follow using these approaches.

Specifically to the processing and assumptions applied here to compute wave-driven renewal metrics, for the French Polynesia region, we suggest several pathways:

1. Having additional validation data for the computations performed here would be useful. In particular, and similar to what Dumas et al. (2012) performed for Ahe, the total inflows estimated through the *hoa* could be compared with the residual (tide-corrected) total outflow in the pass, when a pass is present, or with lagoon water levels when there is no pass (as in Callaghan et al. 2006 for Manihiki Atoll in the Cook Islands).
2. Here, we could only use *hoa* scale flow measurements for validation (Fig. 4), not lagoon-scale. Aucan et al. (2021) suggested a multi-rim relationship at daily scale between wave characteristics and *hoa* inflows that we applied here with a modification for the *C* constant, set to zero, which was a severe choice to limit negative flows. It is likely that more measurements will help refine this critical aspect; especially on type 4 rims (Fig. 2). In this case, for these types of rims, with additional measurement and additional field investigation, the L_{min} and L_{max} characterization of hoa width, and the computed wave-driven flows should be more robust. It is also possible that the Equations 2 to 4 will have to be modified with additional measurements from different locations, with possibly the spatially-explicit tuning of the constants *A* and *C* in Equation 2.

3. Here L_{max} and L_{min} must be understood as geometrical proxy to represent where the minimum and maximum flow transfer occur. One criteria to select the location of the apertures L_{max} and L_{min} is where they will be the most and less efficient respectively (the widest for L_{max}, the narrowest for L_{min}), before the water reaches the lagoon. Hence, their positions closer or further from the crest, can vary with each rim morphology. It is true however, that several interpretations are possible, especially for the structurally complex rims. In itself, the flow dynamics within and across the complex rim should be a field of investigation on its own to enhance the parameterization of the cross-rim flow..
4. We suggest that the WW3 obstruction could be enhanced within the Tuamotu and Gambier archipelagoes, as we have seen a number of inaccurate obstructions, or lack of obstruction (Fig. 3). While the scheme can be considered as efficient enough to work at regional scale (Andréfouët et al. 2012) and around atolls small enough to be truly sub-grid sized, it shows some weaknesses when data are used for atoll scale work and around large atolls. First, the baseline bathymetry needs to be enhanced; and second, adequate obstruction/attenuation needs to be applied, in particular for atolls that cover entirely several cells and which should completely block the incident waves.
5. Other WW3 outputs that are useful for atoll-scale, or even rim-scale work, is to use wave energy partition instead of the peak direction Dp, the peak frequency Fp, and the significant wave height Hs that we have used here. Indeed, the total wave energy signal can be provided in up to five partitions that represent in any given point of the grid the different possible swells crossing that point, ranked by decreasing energy. Each partition has its own direction, frequency and wave height. The peak direction and peak frequency that we used here are the dominant direction and frequency, and Hs (more precisely Hs^2) is the sum of the squares significant wave height of the whole spectrum. Using these peak variables and Hs pose problems if the attenuation due to the obstruction is too weak, as it can allow swells to propagate through an atoll. For instance, we frequently noticed a small tradewind easterlies wave height signal added to wave height of a south or north swell on the west side of a large atoll. This can positively bias the flow estimated for *hoa* on this west side. Hence, WW3 partitions outputs should also be helpful to define more accurate incident swell relative to each rim sector. Altogether, enhancements described here and above (point 4) are likely to avoid overestimating wave height within the archipelago, a likely explanation for the overestimation of the simulated velocities (Fig. 4).
6. To further explore the potential for atoll lagoon classification based on hydrodynamic parameters, in addition to spat collecting statistics that could come from farmers, it would be useful to compare F_{atoll}, *Tr,* or *Tr_s* with chlorophyll a and primary production measurements in a variety of atolls. In Andréfouët et al. (2001b), it was possible to show that *Tr* was related to phytoplankton biomass (chl a) using a series of a few days of measurements in a variety of atolls. Unfortunately, these data from 1994-1998 cannot be revisited here, but in the future, time-series of measurements on a series of contrasted atolls and with replicates within the lagoon would be interesting On-going

measurements using permanent sub-surface probes with in particular fluorimeter chlorophyll data could be useful in the future for this task. Considering existing data sets, a follow-up study will be the linkages between F_{atoll}, Tr, or Tr_s and chlorophyll measurements performed in Ahe, for which there are several time-series and seasonal coverage. (Thomas et al, 2010, Lefebvre et al., 2012). This work will also use the new version of the Ahe 3d hydrodynamic model for comparisons of renewal metrics.

7. When some of these refinements can be applied, we suggest to investigate finely afterwards the causes of the nature of the different periodicities detected on the wavelet analysis, for different atolls. This will require a number of analysis not performed here, including coupling with wind data (Dutheil et al. 2020), origin of the waves (Dutheil et al. 2021), propagation (and obstruction) within the archipelago, and eventually tide-driven processes if the work performed here at daily-scale is extended towards infra-daily processes. It is likely that there will be multiple spatial and temporal scale factors, from local to basin-scales and possibly including an inter-annual ENSO influence.

Eventually, moving towards finer characterizations of high priority atolls in term of resource management using holistic approaches is also highly recommended. Ultimately, high spatial resolution (<100 meter) 3D-model will describe analytically the ensemble of hydrodynamics mechanisms and behaviors responsible for intra-lagoon water quality, trophic potential or spat collecting heterogenenity. Thus far, four atolls have been modeled in a pearl farming context, but more measurements and modelling efforts should eventually replace the type of exploration performed here, albeit with much more time, field data, and funds.

Towards a refined typology of atoll lagoons worldwide

In their review on the oceanic forcing of coral reefs, Lowe and Falter (2014) separated two classes of reefs and atolls with waves and tide-dominated reefs, depending on if the local mean tidal range is greater than the local mean annual significant wave height. Few atolls worldwide can be considered tide-dominated, such as Scott Reef in Western Australia (Green et al. 2018) and most Pacific and Indian Ocean atolls were considered wave-dominated. Some cases, like Ahe atoll, studied in Dumas et al. (2012) could be ambiguous regarding these definitions. The wavelet scalogram of most spat collecting atolls would suggest intermediate classes of atolls than just two. The broad tide-dominated *vs* wave dominated classification is likely to evolve in the future with work that could follow the present analysis. Specifically, atolls studied here show periods where inflows are established by wave-driven process, and periods where this flows is weak or absent. Hence, the notion of tide or wave dominated reefs could be temporally refined based on the spectral statistics of these processes. While tide is not considered here, its effect on lagoon circulation and flushing depends on atoll morphology and can be substantial in French Polynesia when atolsl have a pass (Dumas et al. 2012), and elsewhere

in the Pacific Ocean (Gallagher et al. 1971, Kraines et al. 1999, Rogers et a; 2017). Eventually, tide and its regional variation should be included in the future for a more holistic view of the different types of atolls and forcing, in French Polynesia but also beyond this atoll-rich region. The variability of lagoon answers to different disturbances as well as their potential for economic activities should be better understood with a refined and consistent characterization of their forcing at present time but also in a changing climate era.

Acknowledgements

This study was funded by grant ANR-16-CE32-0004 MANA (Management of Atolls project). MALIS 1 and MALIS 2, two oceanographic cruises in Raroia Atoll on board R/V Alis (https://doi.org/10.17600/18000582), and the POLYPERL cruise in Ahe Atoll also on-board the R/V Alis (https://doi.org/10.17600/13100050) made this work possible. The study was co-funded by the *Direction des Ressources Marines* OTI project, *Contrat de Projet* France-French Polynesia, Program 123, Action 2, 2015-2020. We are also grateful to Raroia's inhabitants for their help during fieldwork. The satellite images used for this study were provided by the *Service de l'Urbanisme de Polynésie française*. The WW3 simulations were performed using HPC resources from GENCI-IDRIS (Grant 2020-A0050107661). The authors also acknowledge the Pôle de Calcul et de Données Marines (PCDM) for providing DATARMOR storage and computational resources (http://www.ifremer.fr/pcdm).

References

Andréfouët, S., Adjeroud, M., 2018. French Polynesia, in: Sheppard, C., (Ed.), World Seas: an Environmental Evaluation, Elsevier. Volume 2 The Indian Ocean to the Pacific, 2, 827–853.

Andréfouët, S., Claereboudt, M., Matsakis, P., Pagès, J., Dufour, P., 2001a. Typology of atoll rims in Tuamotu Archipelago (French Polynesia) at landscape scale using SPOT HRV images. International Journal of Remote Sensing 22, 987–1004.

Andréfouët, S., Pagès, J., Tartinville, B., 2001b. Water renewal time for classification of atoll lagoons in the Tuamotu Archipelago (French Polynesia). Coral Reefs 20, 399–408.

Andréfouët, S., Robinson, J.A., Hu, C., Feldman, G.C., Salvat, B., Payri, C., Muller-Karger, F.E., 2003. Influence of the spatial resolution of SeaWiFS, Landsat-7, SPOT, and International Space Station data on estimates of landscape parameters of Pacific Ocean atolls. Canadian Journal of Remote Sensing 2, 210–218.

Andréfouët S., Chauvin C., Spraggins S.,Torres-Pulliza D, Kranenburg C. 2005, Atlas des récifs coralliens de Polynésie française, Centre IRD de Nouméa, Feb. 2005, pp. 124.

Andréfouët, S., Ouillon, S., Brinkman, R., Falter, J., Douillet, P., Wolk, F., Smith, R., Garen, P., Martinez, E., Laurent, V., Lo, C., Remoissenet, G., Scourzic, B., Gilbert, A., Deleersnijder, E., Steinberg, C., Choukroun, S., Buestel, D., 2006. Review of solutions for 3D hydrodynamic modeling applied to aquaculture in South Pacific atoll lagoons. Marine Pollution Bulletin 52, 1138–1155.

Andréfouët, S., Ardhuin, F., Queffeulou, P., Le Gendre, R., 2012. Island shadow effects and the wave climate of the Western Tuamotu Archipelago (French Polynesia) inferred from altimetry and numerical model data. Marine Pollution Bulletin 65, 415–424.

Andréfouët, S., Dutheil, C., Menkes, C.E., Bador, M., Lengaigne, M., 2015. Mass mortality events in atoll lagoons: environmental control and increased future vulnerability. Global Change Biology 21, 195–205.

Andréfouët, S., Genthon, P., Pelletier, B., Le Gendre, R., Friot, C., Smith, R., Liao, V., 2020. The lagoon geomorphology of pearl farming atolls in the Central Pacific Ocean revisited using detailed bathymetry data. Marine Pollution Bulletin 160, 111580.

Aucan, J., Desclaux, T., Le Gendre, R., Liao, V., Andréfouët, S., 2021. Tide and wave driven flow across the rim reef of the atoll of Raroia (Tuamotu, French Polynesia). Marine Pollution Bulletin 171, 112718.

Battistini, R., Bourrouilh, F., Chevalier, J.-P., Coudray, J., Denizot, M., Faure, G., Fisher, J. C., Guilcher,A.,Harmelin-Vivien,M., Jaubert, J., Laborel, J., Masse, J.-P., Mauge, L. A., Montaggioni, L., Peyrot-Clausade, M., Pichon, M., Plante, R.,Plaziat, J. C., Plessis, Y., Richard, G., Salvat, B., Thomassin, B., Vasseur, P., and Weydert, P., 1975, Eléments de terminologie récifale indopacifique. Thétys, 7, 1-111.

Callaghan, D.P., Nielsen, P., Cartwright, N., Gourlay, M.R., Baldock, T.E., 2006. Atoll lagoon flushing forced by waves. Coastal Engineering 53, 691–704.

Chawla, A., Tolman, H.L., 2008. Obstruction grids for spectral wave models. Ocean Model 22, 12–25.

Chevalier, J.P., 1969. Observations sur les chenaux incomplets appelés hoas dans les atolls des Tuamotu, in: Mar. Bio. Ass (Ed.). Symposium Corals and Coral reef, pp. 477–488.

Deleersnijder E., J.-M. Campin and E.J.M. Delhez, 2001, The concept of age in marine modelling: I. Theory and preliminary model results. Journal of Marine System, 28, 229-267

Delesalle, B., Sournia, A., 1992. Residence time of water and phytoplankton biomass in coral reef lagoons. Continental Shelf Research 12, 939–949.

Delesalle,B., Bell, J., deVaugelas, J., Galzin, R., Rara Moana GIE, 1985. Atoll de Mataiva, archipel des Tuamotu, in: B Delesalle, R Galzin, B Salvat (Eds.), 5th Int. Coral Reef Congress, Tahiti, pp. 269–322.

Desclaux, T., Lemonnier, H., Genthon, P., Soulard, B., Le Gendre, R., 2018. Suitability of a lumped rainfall–runoff model for flashy tropical watersheds in New Caledonia. Hydrological Sciences Journal 63, 1689–1706.

DRM, 2019. Bulletin statistique: Synthèse des données de la pêche professionnelle de l'aquaculture et de la perliculture. Editions 2019. Direction des Ressources Marines de Polynésie française, Papeete, Tahiti, p. 60. (downloaded 30/05/2021 @ www.ressources-marines.gov.pf/bulletin-statistique/)

Dufour, P., Andréfouët, S., Charpy, L., Garcia, N., 2001. Atoll morphometry controls lagoon nutrient regime. Limnol. Oceanogr. 46, 456–461.

Dumas, F., Le Gendre, R., Thomas, Y., Andréfouët, S., 2012. Tidal flushing and wind driven circulation of Ahe atoll lagoon (Tuamotu Archipelago, French Polynesia) from in situ observations and numerical modelling. Marine Pollution Bulletin 65, 425–440.

Dutheil, C., Andréfouët, S., Jullien, S., Le Gendre, R., Aucan, J., Menkes, C., 2020. Characterization of south central Pacific Ocean wind regimes in present and future climate for pearl farming application. Marine Pollution Bulletin 160, 111584.

Dutheil, C., Jullien, S., Aucan, J., Menkes, C., Le Gendre, R., Andréfouët, S., 2021. The wave regimes of the Central Pacific Ocean with a focus on pearl farming atolls. Marine Pollution Bulletin 162, 111751.

Duvall, M.S., Hench, J.L., Rosman, J.H., 2019. Collapsing complexity: quantifying multiscale properties of reef topography. J. Geophys. Res. Oceans 124, 5021–5038.

Gallagher, B., K M Shimada, F I Gonzales, E D Stroup, 1971. Tides and currents in Fanning atoll lagoon. Pacific Science 25, 191–205.

Goldberg, W.M., 2016. Atolls of the World: revisiting the original checklist. Atoll Research Bulletin 610, 1–47.

Green, R.H., Lowe, R.J., Buckley, M.L., 2018. Hydrodynamics of a tidally forced coral reef atoll. J. Geophys. Res. Oceans 123, 7084–7101. h

Jouon, A., Douillet, P., Ouillon, S., Fraunié, P., 2006. Calculations of hydrodynamic time parameters in a semi-opened coastal zone using a 3D hydrodynamic model. Continental Shelf Research 26, 1395–1415.

Kench, P.S., McLean, R.F., 2004. Hydrodynamics and sediment flux of hoa in an Indian Ocean atoll. Earth Surf. Process. Landforms 29, 933–953.

Kraines, S.B., Suzuki, A., Yanagi, T., Isobe, M., Guo, X.Y., Komiyama, H., 1999. Rapid water exchange between the lagoon and the open ocean at Majuro Atoll due to wind, waves, and tide. J. Geophys. Res.-Oceans 104, 15635–15653.

Labat, D. Recent advances in wavelet analyses: Part 1. A review of concepts. Journal of Hydrology 314, 275–288 (2005).

Laurent, V., Varney, P., 2014. Historique des cyclones de Polynésie française de 1831 à 2010. Meteo France, Papeete. 172 p.

Lefebvre, S., Claquin, P., Orvain, F., Véron, B., Charpy, L., 2012. Spatial and temporal dynamics of size-structured photosynthetic parameters (PAM) and primary production (13C) of pico- and nano-phytoplankton in an atoll lagoon. Marine Pollution Bulletin 65, 478–489.

Lenhardt, X., 1991. Hydrodynamique des lagons d'atolls et d'ile haute en Polynésie Française. PhD Thesis. Mus. Nat. Histoire Nat., Paris. p. 132.

Leonard, N.D., Welsh, K.J., Lough, J.M., Feng, Y. X., Pandolfi, J.M., Clark, T.R., Zhao, J., 2016. Evidence of reduced mid-Holocene ENSO variance on the Great Barrier Reef, Australia: Paleoceanography 31, 1248–1260.

Lowe, R.J., Falter, J.L., 2015. Oceanic Forcing of Coral Reefs. Annu. Rev. Mar. Sci. 7, 43–66.

Lucas, L.V., Deleersnijder, E., 2020. Timescale Methods for Simplifying, Understanding and Modeling Biophysical and Water Quality Processes in Coastal Aquatic Ecosystems: A Review. Water 12, 2717.

Massel, S.R., 2001. Wavelet analysis for processing of ocean surface wave records. Ocean Engineering 28, 957–987.

Montaggioni, L.F., Pirazzoli, P.A., 1984. The significance of exposed coral conglomerates from French Polynesia (Pacific Ocean) as indicators of recent relative sea-level changes. Coral Reefs 3, 29–42. https://doi.org/10.1007/BF00306138

Newell, N., 1956. Geological reconnaissance of Raroia (Kon-tiki) atoll, Tuamotu archipelago. Bulletin of the American Museum of Natural History 109, 311–372.

Onderka, M., Chudoba, V., 2018. The Wavelets show it – the transit time of water varies in time. Journal of Hydrology and Hydromechanics 66, 295–302.

Pagès, J., Andréfouët, S., 2001. A reconnaissance approach for hydrology of atoll lagoons. Coral Reefs 20, 409–414.

Purdy, E.G., E L Winterer, 2001. Origin of atoll lagoons. Geological Society America Bulletin 113, 837–854.

Rodier, M., Longo, S., Henry, K., Ung, A., Lo-Yat, A., Darius, H., Viallon, J., Beker, B., Delesalle, B., Chinain, M., 2019. Diversity and toxic potential of algal bloom-forming species from Takaroa

lagoon (Tuamotu, French Polynesia): a field and mesocosm study. Aquat. Microb. Ecol. 83, 15–34.

Rogers, J.S., Monismith, S.G., Fringer, O.B., Koweek, D.A., Dunbar, R.B., 2017. A coupled wave-hydrodynamic model of an atoll with high friction: Mechanisms for flow, connectivity, and ecological implications. Ocean Modelling 110, 66–82.

Salvat, B., 1985. An integrated (geomorphological and economical) classification of French Polynesian atolls. In: Delesalle B, Galzin R, Salvat B (eds) Proc Fifth Int Coral Reef Congr, Tahiti, 2, 337

Sangare, N., Lo-Yat, A., Le Moullac, G., Pecquerie, L., Thomas, Y., Beliaeff, B., Andréfouët, S., 2019. Estimation of physical and physiological performances of blacklip pearl oyster larvae in view of DEB modeling and recruitment assessment. Journal of Experimental Marine Biology and Ecology 512, 42–50.

Smith, L., Turcotte, D., Isacks, B., 1998. Stream flow characterization and feature detection using a discrete wavelet transform. Hydrological Processes 12, 233-249.

Stoddart, F R Fosberg, 1994. The hoa of Hull atoll and the problem of hoa. Atoll Research Bulletin 394, 1–26.

Tartinville, B., Rancher, J., 2000. Wave-Induced Flow over Mururoa Atoll Reef. Journal of Coastal Research 16, 7.

Tartinville, B., Deleersnijder, E., Rancher, J., 1997. The water residence time in the Mururoa atoll lagoon: Sensitivity analysis of three-dimensional model. Coral-Reefs 16, 193–203.

Teague, W.J., Wijesekera, H.W., Jarosz, E., Lugo-Fernández, A., Hallock, Z.R., 2014. Wavelet analysis of near-inertial currents at the East Flower Garden Bank. Continental Shelf Research 88, 47–60.

Thomas, Y., Garen, P., Courties, C., Charpy, L., 2010. Spatial and temporal variability of the pico- and nanophytoplankton and bacterioplankton in a deep Polynesian atoll lagoon. Aquat. Microb. Ecol. 59, 89–101.

Thomas, Y., Dumas, F., Andréfouët, S., 2016. Larval connectivity of pearl oyster through biophysical modelling; evidence of food limitation and broodstock effect. Estuarine, Coastal and Shelf Science 182, 283–293.

Tolman, H.L., 2009. User Manual and System Documentation of WAVEWATCH III TM Version 3.14. 220.

Torrence, C., Compo, G. P. 1998: A practical guide to wavelet analysis. Bull. Amer. Meteor. Soc., 79, 61–78.

Valle-Levinson, A., Kourafalou, V.H., Smith, R.H., Androulidakis, Y., 2020. Flow structures over mesophotic coral ecosystems in the eastern Gulf of Mexico. Continental Shelf Research 207, 104219.

Woodroffe, C.D., Biribo, N., 2011. Atolls. In: Hopley, D. (Ed.), Encyclopedia of Modern Coral Reefs, Structure, Form and Process. Springer Science+Business Media BV, Dordrecht, Netherlands, pp. 51–71.

*Table 1: Main parameters for the 74 processed atolls. Atolls written in bold are the main pearl farming atolls as in 2019 (DRM, 2019). This may not represent the status of the past 30 years since pearl farming may have stopped recently in some atolls. ** Highly productive spat collecting atolls. * Moderately productive spat collecting atolls. Per.=perimeter; Vol.=volume. Lmin and Lmax are defined in the text. Here, the sum over the atoll is provided. Area is the surface area of the lagoon (not the entire atoll). Sector is the number of sectors around each atoll (each sector is related to only one cell of the WW3 grid).Ap_{min} is the ratio between Per and L_{min}. Ap_{max} is the ratio between Per and L_{min}. Ap% is the percentage of increase of aperture from L_{min}.to L_{max}.*

Atoll	Archipelago	Latitude	Longitude	Per. (km)	Area (km^2)	Vol. (km^3)	Sectors	L_{min} (m)	L_{max} (m)	A
Ahe**	Tuamotu	-146.301	-14.483	58.46	140.92	5,82	9	2374	7489	
Amanu	Tuamotu	-140.755	-17.800	74.13	208.92		11	6039	20705	
Anaa	Tuamotu	-145.491	-17.413	70.20	91.14		9	5357	14329	
Anuanuraro	Tuamotu	-143.535	-20.435	16.68	6.77		5	639	3000	
Anuanurunga	Tuamotu	-143.286	-20.615	9.73	2.07		4	220	5009	
Apataki*	Tuamotu	-146.308	-15.445	109.23	678.45		8	13902	36162	
Aratika*	Tuamotu	-145.533	-15.537	60.63	147.48		8	6325	21184	
Arutua	Tuamotu	-146.737	-15.310	92.89	504.80		9	16799	44643	
Faaite	Tuamotu	-145.215	-16.753	68.52	222.08		9	8357	34922	
Fakahina	Tuamotu	-140.133	-15.983	22.39	17.59		5	157	1243	
Fakarava	Tuamotu	-145.585	-16.306	165.02	1096.43		6	5342	77700	
Fangatau	Tuamotu	-140.864	-15.826	20.33	7.86		6	1781	6781	
Hao	Tuamotu	-140.884	-18.230	136.44	490.65		16	12548	44472	
Haraiki	Tuamotu	-143.450	-17.467	21.54	10.08		6	1270	4879	
Hereheretue	Tuamotu	-144.957	-19.870	27.59	27.14		6	3976	11606	
Hikueru	Tuamotu	-142.614	-17.592	39.83	78.77		9	7812	17491	
Hiti	Tuamotu	-144.094	-16.726	19.04	14.29		7	2270	7257	
Katiu*	Tuamotu	-144.364	-16.423	66.46	228.73		8	7753	27053	
Kauehi	Tuamotu	-145.159	-15.878	73.10	305.94		10	4523	15340	
Kaukura	Tuamotu	-146.698	-15.751	109.72	414.81		9	30289	74173	
Makemo	Tuamotu	-143.682	-16.618	167.14	585.25		15	26253	87363	
Manihi**	Tuamotu	-145.930	-14.398	67.13	161.15		7	2717	8175	
Manuhangi	Tuamotu	-141.243	-19.202	15.06	8.19		4	134	882	
Marokau	Tuamotu	-142.270	-18.052	100.32	212.05		12	8814	25530	
Marutea nord	Tuamotu	-143.108	-17.046	109.22	446.53		10	40476	76406	
Mataiva	Tuamotu	-148.667	-14.884	27.52	12.13		4	251	952	
Motutunga	Tuamotu	-144.364	-17.105	48.75	123.56		8	4971	30137	
Napuka	Tuamotu	-141.232	-14.172	27.56	18.93		6	2400	5486	
Nengonengo	Tuamotu	-141.804	-18.753	38.43	66.37		6	1901	11622	
Nihiru	Tuamotu	-142.834	-16.692	45.10	73.47		14	8448	12001	
Nukutepipi	Tuamotu	-143.052	-20.699	9.54	0.93		4	816	2621	
Paraoa	Tuamotu	-140.690	-19.135	18.70	15.14		5	700	3593	
Pinaki	Tuamotu	-138.675	-19.395	7.08	0.47		5	49	144	
Puka Puka	Tuamotu	-138.809	-14.820	17.73	1.95		4	233	552	
Pukarua	Tuamotu	-137.017	-18.312	35.26	27.84		4	884	7601	
Rangiroa	Tuamotu	-144.890	-16.176	206.51	1574.15		10	15255	70960	
Raraka	Tuamotu	-142.422	-16.074	75.74	353.60	11,86	9	3938	23971	
Raroia*	Tuamotu	-142.149	-18.234	93.70	348.12		10	10037	26374	
Ravahere	Tuamotu	-136.377	-18.512	49.50	44.44		11	1771	20793	
Reao	Tuamotu	-143.075	-17.854	49.21	38.33		8	291	6581	
Reitoru	Tuamotu	-141.922	-16.834	14.61	5.14		5	331	5555	
Rekareka	Tuamotu	-147.623	-15.140	8.97	0.69		4	56	247	
Taenga	Tuamotu	-143.131	-16.358	64.98	166.83		8	4463	24659	
Tahanea	Tuamotu	-144.740	-16.886	117.29	535.81		9	22352	67032	

Takapoto**	Tuamotu	-145.201	-14.621	49.50	76.54	1,95	10	253	1575
Takaroa**	Tuamotu	-144.979	-14.458	61.52	85.26	2,22	8	1073	3560
Takume*	Tuamotu	-142.207	-15.809	47.17	40.44	0,83	6	5245	18752
Tatakoto	Tuamotu	-138.395	-17.349	30.96	16.78		2	2074	5563
Tauere	Tuamotu	-141.507	-17.377	15.63	7.54		5	534	2534
Tekokota	Tuamotu	-142.573	-17.312	10.57	4.70		8	3449	6061
Tepoto sud	Tuamotu	-144.281	-16.820	9.55	1.34		6	368	1378
Tikehau	Tuamotu	-148.174	-15.004	80.14	382.82		8	6212	23372
Toau	Tuamotu	-146.039	-15.908	104.58	549.18		8	33392	53403
Tuanake	Tuamotu	-144.213	-16.653	24.52	24.79		6	1667	6485
Vahitahi	Tuamotu	-138.811	-18.772	19.25	7.45		5	1719	6060
Vairaatea	Tuamotu	-139.219	-19.349	18.62	12.69		5	433	3461
Fangataufa	Gambier	-138.738	-22.233	30.29	34.33		8	191	842
Maria	Gambier	-136.189	-22.012	14.34	6.55		4	61	342
Marutea Sud*	Gambier	-135.566	-21.524	55.51	108.03		5	8746	17246
Matureivavao	Gambier	-136.394	-21.468	18.78	16.81		7	850	5599
Morane	Gambier	-137.133	-23.154	16.11	9.22		14	1055	7064
Moruroa	Gambier	-138.878	-21.836	66.65	130.51	4,5	12	9222	16185
Tematangi	Gambier	-140.628	-21.678	38.63	59.48		8	988	3226
Temoe	Gambier	-134.479	-23.343	19.33	13.02		8	843	3372
Tenararo	Gambier	-136.745	-21.303	8.96	1.74		5	54	224
Tenarunga	Gambier	-136.542	-21.343	12.95	5.82		4	12	150
Tureia	Gambier	-138.539	-20.829	19.33	57.73		5	196	795
Vahanga	Gambier	-136.650	-21.330	12.06	4.86		6	116	477
Vanavana	Gambier	-139.141	-20.780	9.54	2.39		4	11	78
Bellinghausen	Society	-154.524	-15.814	12.87	2.83		5	2091	2814
Mopelia	Society	-153.956	-16.812	28.22	28.74	0,75	7	9109	14375
Scilly	Society	-154.685	-16.542	42.99	80.66		9	4119	18111
Tetiaroa	Society	-149.556	-17.005	25.70	10.76		8	5393	11692
Tupai	Society	-151.817	-16.253	24.63	7.81		6	348	601